IEEE Access
Multidisciplinary ⋮ Rapid Review ⋮ Open Access Journal

Received 11 October 2023, accepted 25 October 2023, date of publication 31 October 2023, date of current version 7 November 2023.

Digital Object Identifier 10.1109/ACCESS.2023.3328958

RESEARCH ARTICLE

Optimal Power Flow Analysis With Renewable Energy Resource Uncertainty: A Hybrid AEO-CGO Approach

MOHAMED H. HASSAN[1], SALAH KAMEL[2], AYOOB ALATEEQ[3], ABDULLAH ALASSAF[3], AND IBRAHIM ALSALEH[3], (Member, IEEE)

[1]Ministry of Electricity and Renewable Energy, Cairo 11517, Egypt
[2]Department of Electrical Engineering, Faculty of Engineering, Aswan University, Aswan 81542, Egypt
[3]Department of Electrical Engineering, College of Engineering, University of Hail, Hail 55211, Saudi Arabia

Corresponding author: Salah Kamel (skamel@aswu.edu.eg)

This work was supported by the Scientific Research Deanship at University of Hail, Saudi Arabia, under Project RG-23 172.

ABSTRACT Over the last decade, significant advancements have occurred in global electricity networks due to the widespread adoption of renewable energy resources (RES). While these sources offer numerous benefits such as cost-effective operation of solar photovoltaic and wind power stations and reduction of environmental hazards related to traditional power sources, they have also introduced various challenges to power network scheduling and operation. The traditional optimal power flow (OPF) problem, which is inherently complex, has become even more intricate with the integration of RES alongside traditional thermal power generators. This complexity arises from the unpredictable and intermittent nature of those resources. To tackle the intricacies of incorporating RES into conventional electric power systems, this study utilizes a pair of probability distribution functions to predict the power generation of wind and solar PV systems, respectively. The comprehensive OPF, which includes RES components, is expressed as a singular objective problem encompassing multiple goals including reducing fuel costs, emissions, real transmission losses, and voltage deviations. To tackle this challenge, a novel hybrid metaheuristic optimization algorithm (ACGO) is introduced. The ACGO algorithm combines Chaos game optimization (CGO) with the artificial ecosystem-based optimization (AEO) method to obtain the optimum solution for the OPF problem considering stochastic RES. This technique aims to enhance solution precision by increasing solution diversity through an optimization process. The modified optimizer's validation begins by examining its performance using well-known benchmark optimization functions, demonstrating its superiority over CGO, AEO, and other competitive algorithms. Subsequently, the modified optimizer is applied to a combined model of a wind and PV-incorporated IEEE 30-bus system. The ACGO technique proves to be highly effective, yielding the lowest fitness values of 781.1675 \$/h and 808.4109 \$/h in their respective scenarios for the modified IEEE 30-bus system. Additionally, the proposed ACGO method achieves the optimal total cost of 31623.5 \$/h and 31601.55 \$/h for the modified IEEE 57-bus system. These results emphasize the accuracy and robustness of ACGO in effectively addressing various instances of the OPF problem. The performance of ACGO in solving the OPF issue is verified through statistical boxplot comparisons, non-parametric tests, and robustness analyses. The evaluations indicate that the ACGO technique outperforms other well-known optimization algorithms in achieving the optimum values for the OPF problem involving stochastic PV and wind power systems. Additionally, the results show that ACGO offers faster convergence rates and higher precision in convergence compared to conventional artificial ecosystem-based optimization, Chaos game optimization, and other recent heuristic, metaheuristic, and hybrid optimization algorithms. The effectiveness of the ACGO technique has been proven to be robust and efficient, making it suitable for multidisciplinary problems and engineering optimization challenges.

The associate editor coordinating the review of this manuscript and approving it for publication was Fabio Mottola.

INDEX TERMS Optimal power flow, stochastic renewable energy sources, artificial ecosystem-based optimization, chaos game optimization.

NOMENCLATURE

RES	Renewable energy sources.
AEO	Artificial ecosystem-based optimization.
GBO	Gradient-based optimizer.
WT	Wind turbines.
VPLE	Valve Point Loading Effect.
MFO	Moth flame optimization.
HPO	Hunter–prey optimizer.
NGO	Northern Goshawk Optimization.
PDF	Probability density function.
STD	Standard deviation.
ESMA	Enhanced Slime Mould Algorithm.
WSA	White Sharks Algorithm.
EHPO	Enhanced Hunter-prey optimization.
DEEPSO	Differential evolutionary particle swarm optimization.
CFPA	Chaotic flower pollination algorithm.
HHO	Harris Hawks optimization.
GOA	Grasshopper optimization algorithm.
GWO	Grey wolf optimizer.
CSA	Crow search algorithm.
ABC	Artificial bee colony algorithm.
JS	Jellyfish search (JS) optimizer.
GPC	Giza pyramids construction.
FPA	Flower pollination algorithm.
GTO	Gorilla troops optimization.
OPF	Optimal power flow.
CGO	Chaos game optimization.
SPV	Solar photovoltaics.
ML	Machine learning.
CT	Carbon Tax.
EEO	Enhanced equilibrium optimizer.
TSO	Transient search optimization.
HPO	Hunter-prey optimization.
EO	Equilibrium Optimizer.
SSA	Salp Swarm Algorithm.
WHO	Wild Horse Optimizer.
ACGO	Hybrid AEO-CGO algorithms.
MPSO	Mutation-based particle swarm optimization.
EES	Elite evolutionary strategy.
FACTS	Flexible Alternating Current Transmission Systems.
WRST	Wilcoxon rank-sum test.
BWOA	Black widow optimization algorithm.
ALO	Ant lion optimizer.
GSA	Gravitational search algorithm.
BMO	Barnacles mating optimizer.
TLBO	Teaching-learning-based optimization.
IEO	Improved Equilibrium Optimizer.
HGS	Hunger games search.
OPA	Orca predation algorithm.

I. INTRODUCTION

A. BACKGROUND

The urgent need to reduce fuel costs in traditional power generation facilities and mitigate greenhouse gas emissions from thermal power generators has prompted numerous electric power companies to transition towards harnessing renewable energy sources. Moreover, advancements in renewable energy technologies have played a crucial role in establishing them as the most cost-effective and environmentally conscious options. The strategic integration of wind and solar photovoltaic (SPV) systems in well-suited locations, combined with optimal adjustments to conventional power network parameters, can significantly influence the effectiveness of power system control and operation. In order to enhance accuracy and authenticity of wind and SPV modeling, the utilization of the Weibull probability distribution function for wind speed prediction has been documented [1], while previous research has employed the lognormal probability distribution function for simulating the sporadic nature of solar irradiance [2].

B. LITERATURE REVIEW

In the realm of contemporary electrical power system design, the OPF stands as a foundational optimization challenge that has persisted over numerous years and remains of paramount significance to the current era. The OPF represents a notable non-convex and nonlinear conundrum, with its primary objective being the refinement of control parameters to attain optimal values. This pursuit is aimed at the dual goal of diminishing fuel expenses and power losses, all while accommodating a multitude of diverse equality and inequality restrictions within a given power system framework [3]. A multitude of works within the academic literature have delved into the examination of the Optimal Power Flow (OPF) dilemma within systems encompassing both conventional and renewable energy sources. The primary focus of this quandary centers on the identification of optimal configurations for control parameters. These configurations aim to optimize specific objective functions, which may encompass factors including fuel costs, emissions expenditures, transmission losses, and voltage profiles. All the while, these sought-after optimizations must conform to a predefined array of functioning and physical limitations. Notably, the control variables of the OPF predicament involve various aspects, including the effective power outputs at unit nodes (without the slack bus), voltage magnitudes at all unit nodes, transformer tap changers, and shunt compensators.

A diverse array of conventional optimization techniques has successfully addressed issues related to OPF concerns. These techniques, predominantly reliant on derivatives and gradient approaches like non-linear and quadratic programming [4], exhibit remarkable convergence properties. However, their utility is tempered by several shortcomings. They struggle to identify global solutions in the presence of non-convexity and encounter challenges when tackling problems involving non-differentiable and discontinuous objective functions. More recently, there has been a surge in interest surrounding metaheuristic optimization algorithms. These algorithms are captivating due to their adaptability, absence of dependence on derivatives, and ability to circumvent local optima. Over the past few decades, these metaheuristic algorithms have been cultivated, drawing inspiration from physical phenomena, animal actions, and evolutionary principles. They offer direct and efficient resolutions to the aforementioned problems.

An investigation was conducted into a novel hybrid approach, termed the Gradient-Based optimization algorithm based on moth flame Optimization (GBO-MFO) approach. This method seeks to detect optimum positioning and dimensions of FACTS devices within an altered power system. The system takes into account stochastic wind sources and conventional thermal power plants, all within the context of the OPF. The GBO-MFO approach was employed to choose the most appropriate location and suitable sizing for FACTS devices. This task was accomplished by expressing a multi-objective function that encompasses two critical aspects: the cost of maintaining reserves to account for potential overestimations and penalties incurred for underestimating intermittent renewable sources. Additionally, the algorithm considered the minimization of active transmission losses as part of the optimization process [5]. A rising and significant effort has been made in recent years to model and attain the optimal results for the OPF problem as well as RES. The OPF problem with considering uncertainties in the PV energy, wind, and load prediction and improved by a hybrid optimization technique according to a machine learning (ML) method and transient search optimizer (TSO) (ML-TSO) algorithm is presented in [6]. The classical and probabilistic OPF problem for two large-scale power networks (IEEE 57-bus, and IEEE 118-bus) was solved by a ML-TSO. The results demonstrated the strength and efficacy of the ML-TSO approach to solve the OPF problems.

An enhanced hunter-prey optimization (EHPO) approach in [7] was suggested to tune the parameters of a FACTS devices and optimize OPF, with wind and solar power. Moreover, it is confirmed that EHPO is robustness to achieve the global search exploration than the conventional hunter-prey optimization (HPO) and the HPO algorithm as well does not success during attaining the optimum solution for the large-scale power systems. A hybrid Harris hawks optimization method (HHO) to the incorporation of RES is proposed in [8]. An optimum reactive power dispatch with considering uncertainties PV power and its influence on reducing the active transmission losses is optimized by the Rao-3 technique for addressing this problem [9]. The Rao-3 algorithm was confirmed by three standard test power systems. AEO algorithm has been applied for the large scale optimal reactive power dispatch problem [10]. OPF problems incorporating intermittent sources was solved using slim mould optimizer [11]. Gorilla troops optimization (GTO) technique was used to achieve best solution for the OPF considering uncertainty of RES [12]. Hybrid wind PV power systems are addressed by the differential evolutionary PSO (DEEPSO) that can perform probabilistic OPF with high precision [13]. Indeterminate wind speed and solar irradiance were simulated using Rayleigh probability and log-normal distributions. The fuel cost, fuel cost with VPLE, emission, active power losses, and voltage deviation are minimized and optimized using an improved equilibrium optimizer (EO), known as EEO algorithm. This method has numerous benefits, such as simple encoding, integer discrete handling, rapid convergence, and high-quality feasible solutions for various OPF issues [14]. Besides, OPF problem is optimized by an enhanced version of the salp swarm algorithm (SSA) called ISSA technique [15].

A modified Rao-2 (MRao-2) technique is applied to find the best solution for OPF, as well as wind and solar. The primary objective of the OPF's fitness function is to minimize fuel costs across various scenarios. In the context of the IEEE 30-bus system, it seeks to reduce fuel costs in 3 study cases: without and with Renewable Energy resources, and with RES under contingency conditions. Meanwhile, for the IEEE 118-bus system, the fitness function focuses on fuel cost reduction in 2 cases: without and with RES [16]. The OPF, considering the wind and solar power, is modeled and optimized based on a mutation-based particle swarm optimization (MPSO) approach. Solar radiation and wind speed were supposed to find the normal and Weibull distributions and the uncertainty was executed by Monte-Carlo method [17]. An elite evolutionary strategy (EES) based on evolutionary methods to enhance the Wild Horse Optimizer (WHO), forming an improved hybrid algorithm called EESWHO is solved and optimized the OPF considering uncertainties PV power and wind. The prediction solar PV and wind are modeled by lognormal and Weibull probability distribution functions [18]. The constrained OPF problem participating a hybrid solar PV and wind power for IEEE 30-bus, 57-bus, and 118-bus is addressed by an enhanced chaotic flower pollination algorithm (CFPA) [19]. This method can successfully to enhance the search competence, variety, and convergence rate.

C. CONTRIBUTION AND PAPER ORGANIZATION

Artificial Ecosystem-based Optimization (AEO) [20], and chaos game optimizer (CGO) [21] techniques are both potent and robust population-based metaheuristic algorithms. They draw inspiration from different aspects of nature: AEO is inspired by the energy flow within Earth's ecosystem, while CGO incorporates principles of chaos theory, utilizing fractal arrangements through the chaos game concept and addressing self-similarity challenges in fractals. While CGO offers advantages such as easy implementation and strong adaptability, it faces difficulties in escaping local optima once trapped in them. Similarly, like many other optimization methods, both AEO and CGO begin by generating an initial population of solutions randomly within the problem space [22]. Subsequently, these solutions undergo updates based on historical data and information derived from alternative solutions within a confined number of iterations [23]. Through this gradual progression, the solutions' quality is enhanced, leading to the discovery of more optimal solutions for the given problem. These algorithms have been deployed across diverse problem domains and subjected to rigorous testing using a multitude of test functions, yielding promising outcomes. Nevertheless, they exhibit certain limitations. For instance, their convergence rate proves inadequate for certain high-dimensional and intricate issues, and they do not assure a definitive optimal solution within a reasonable timeframe. Furthermore, the AEO algorithm demonstrates limited exploratory capacity and suboptimal performance in scenarios involving multiple modes. Additionally, susceptibility to local optima hampers their effectiveness. Once trapped in a local optimum, these algorithms lack the ability to explore other regions of the problem space with extended iterations. This remark proves especially detrimental when applied to real-world NP-Hard applications. Addressing the aforementioned deficiencies and others requires a significant endeavor in conceiving and advancing novel optimization algorithms, presenting an ongoing challenge. Academics have provided several methods to deal with these weaknesses, such as having benefit of the chaos concept [24], [25], utilizing of orthogonal learning [26], [27], hybridizing supplementary algorithms [28], [29], employing oppositional learning [30], [31], using a quantum-based strategy [32], [33], etc.

This article aims to address the limitations of the original AEO and CGO techniques by proposing a hybrid metaheuristic optimization algorithm called ACGO. The ACGO algorithm is suggested as a solution to overcome the limitations and optimize the OPF problem with incorporated renewable energy sources (RES). This enhancement in the ACGO technique enhances its exploration capability compared to the AEO and CGO algorithms. Moreover, the ACGO method's exploration capability remains unaffected by the number of iterations, preventing it from getting stuck in local minima solutions. The ACGO technique is verified on the improved IEEE 30-bus with RESs and simulation results are compared with many recent techniques. The main contributions of this paper are summarized in these points:

- ✓ Proposing the hybrid metaheuristic optimization technique (ACGO) as a means to enhance exploration capabilities and prevent entrapment in local optima zones.
- ✓ Introducing a novel application of the AEO, CGO, and ACGO methodologies to achieve optimal solutions for the OPF problem, taking into consideration the incorporation of uncertainty models for RESs.
- ✓ The fitness function outlined in this research encompasses the generation cost of the conventional thermal units, accompanied by the direct, reserve, and penalty costs attributed to WT and SPV generators. Additionally, an investigation into the influence of changing reserve and penalty costs on the optimum configuration is conducted.
- ✓ The statistical outcomes obtained through the proposed algorithm are juxtaposed against those of traditional AEO and CGO techniques, as well as other widely recognized methods.
- ✓ The efficacy and consistency of the ACGO approach in addressing the optimal power flow problem, while accommodating uncertainty models for RESs, are duly substantiated.

The rest of this paper is divided into the following sections that are obviously itemized as follows: Section II introduce the OPF's mathematical formulation and operating restrictions, Section III describes the models of WT and SPV units' output. The original AEO, CGO and the ACGO technique is presented in section IV. In Section V, the ACGO approach is applied for achieving the best solution for the 23 benchmark functions and the OPF problem with the existence of RESs, also showing the attained results. Section VI summarizes the main work's conclusions.

II. THE CALCULATED MODEL OF THE OPF

The OPF is a complicated and non-linear problem in the field of power system engineering and solving the OPF problem effectively is a critical task in power system operation and planning. The solving of OPF depends on defining the optimum value of the control variables that reduce the fitness function, taking into consideration several operating constraints. The essential fitness function of this article is decreasing the total generating cost which contains the fuel cost of the thermal generators without or with RESs units' outputs. Moreover, the optimum control variables are the active and reactive of the units and voltages, shunt VAR capacitors, and transformer tap ratio.

A. FUEL COST FOR THE THERMAL UNITS

Fuel cost is a critical factor in the operation and optimization of thermal power units within the framework of OPF in the field of electrical engineering and power systems. Thermal units operate using fossil fuels, and the cost of fuel is determined as follows [14]:

$$F(P_{cg}) = \sum\nolimits_{i=1}^{N_g} \alpha_i P_{cg,i}^2 + \beta_i P_{cg,i} + \gamma_i \tag{1}$$

where F denotes to the fuel cost, N_g represents the total number of the conventional units, $P_{cg,i}$ is the active power produced from unit i. α_i, β_i, and γ_i refer to the cost's coefficients based on the i-th thermal generators. Though, with taking into consideration VPLE, the quadratic fuel cost become specific with further accurate [34]. Subsequently, the cost function based on the multi-valve loading effect is presented as follows [35]:

$$F(P_{cg}) = \sum\nolimits_{i=1}^{N_g} \alpha_i P_{cg,i}^2 + \beta_i P_{cg,i} + \gamma_i + \Big|e_i \times \sin\left(g_i(P_{cg,i}^{min} - P_{cg,i})\right)\Big| \tag{2}$$

e_i and g_i are the i-th thermal unit's valve point cost coefficients of, and $P_{cg,i}^{min}$ is the minimum real power that the i-th thermal units generates.

B. THE COST OF WT AND SOLAR PV UNITS

Wind Turbine and solar PV units do not require fuel in order to the operation and only require primary maintenance or expenditure costs [34]. The energy generated from RES that is scheduled according to the jointly contracted agreement. The direct cost of SPV and WT units is associated with private parties and can be defined as follows:

$$C_{W_j}\left(P_{W_{s,j}}\right) = g_{W_d} P_{W_{s,j}} \tag{3}$$

where C_{W_j} represents the direct cost of the j-th WT unit, g_{W_d} is the direct cost's coefficient for the WT unit, while $P_{W_{s,j}}$ is the scheduled generation of the j-th wind unit. Furthermore, the calculation of the direct cost associated with the k-th SPV unit in relation to its scheduled power is mathematically performed in the following equation [18]:

$$C_{S_k}\left(P_{S_{s,k}}\right) = g_{S_d} P_{S_{s,k}} \tag{4}$$

where g_{S_d} represents the the SPV unit's direct cost coefficient, while $P_{S_{s,k}}$ refers to the scheduled generation of the k-th solar PV unit.

C. COST CALCULATION OF WT UNITS

Regarding the power of RESs, two scenarios will arise. The first scenario occurs while the RESs generate more power than expected, known as "underestimated output power." In this situation, there is a risk of excess power going to waste. To mitigate this concern, power grid operators' goal to decrease the output from thermal units, incurring a cost denoted to as the "penalty cost." This cost is incurred using the operators of this system for the surplus power generated by WT generators and is expressed as follows [18]:

$$\begin{aligned} C_{U_{w,j}}\left(P_{W_{a,j}} - P_{W_{s,j}}\right) &= p_{W,j}\left(P_{W_{a,j}} - P_{W_{s,j}}\right) \\ &= p_{W,j}\int_{P_{W_{s,j}}}^{P_{W_{r,j}}}\left(P_{W,j}\right. \\ &\left. -P_{W_{s,j}}\right) F_W\left(P_{W,j}\right) dP_{W,j} \end{aligned} \tag{5}$$

where $P_{W_{a,j}}$, and $P_{W_{s,j}}$, refer to the accessible, schedule output power from j-th WT unit, respectively and $P_{W_{r,j}}$ denotes the rated output power of the j-th WT unit. $p_{W,j}$ is the coefficient of the penalty cost for the j-th WT generator and $F_W\left(P_{W,j}\right)$ denote the PDF of produced power of the j-th WT unit.

The second case arises while the power of RES falls short of the predictable value, referred to as "overestimated output power." In order to mitigate this state, the system operators should assign spinning reserves to thermal units to recompense for the overestimated power of the RES and confirm uninterrupted power supply for the whole customers. The expense associated with maintaining these power reserves is termed the "reserve cost" and can be computed using the following equation [18]:

$$\begin{aligned} C_{O_{W,j}}\left(P_{W_{s,j}} - P_{W_{a,j}}\right) &= R_{W,j}\left(P_{W_{s,j}} - P_{W_{a,j}}\right) \\ &= R_{W,j}\int_{0}^{P_{W_{s,j}}}\left(P_{W_{s,j}}\right. \\ &\left. -P_{W_{a,j}}\right) F_W\left(P_{W,j}\right) dP_{W,j} \end{aligned} \tag{6}$$

where $R_{W,j}$ is coefficient the reserve cost for the j-th WT unit. Additionally, the produced power probability determination of several WT units at various wind speeds.

D. COST CALCULATION OF SPV UNITS

Furthermore, the electricity generated by SPV units for the grid is inherently uncertain. The approach used to address underestimation and overestimation of solar PV units is akin to that employed to WT units, with the key difference being the modeling of solar radiation using a lognormal probability distribution function (PDF). The penalty cost for the k-th SPV generator is defined as follows [18]:

$$\begin{aligned} C_{U_{S,K}}\left(P_{S_{a,K}} - P_{S_{s,K}}\right) &= p_{S,K}\left(P_{S_{a,K}} - P_{S_{s,K}}\right) \\ &= p_{S,K}\cdot F_S\left(P_{S_{a,K}} > P_{S_{s,K}}\right) \\ &\cdot \left[E\left(P_{S_{a,K}} > P_{S_{s,K}}\right) - P_{S_{s,K}}\right] \end{aligned} \tag{7}$$

where $P_{S_{a,K}}$ and $P_{S_{s,j}}$ refer to the existing and schedule power of the K-th SPV unit, respectively, $p_{S,K}$ refers to the coefficient of the penalty cost relating to the K-th SPV units, $F_S\left(P_{S_{a,K}} > P_{S_{s,K}}\right)$ is the probability of surplus power produced using the k-th SPV unit compared to $P_{S_{a,K}}$, and $E\left(P_{S_{a,K}} > P_{S_{s,K}}\right)$ denotes the expectable surplus output power. In the overestimation case, the reserve cost is assessed from the following equation [18]:

$$\begin{aligned} C_{O_{S,K}}\left(P_{S_{s,K}} - P_{S_{a,K}}\right) &= R_{S,K}\left(P_{S_{s,K}} - P_{S_{a,K}}\right) \\ &= R_{S,K}\cdot F_S\left(P_{S_{a,K}} < P_{S_{s,K}}\right)\cdot\left[P_{S_{s,K}}\right. \\ &\left. - E\left(P_{S_{a,K}} < P_{S_{s,K}}\right)\right] \end{aligned} \tag{8}$$

where $R_{S,K}$ denotes the reserve cost's coefficient for the K-th SPV unit, $F_S\left(P_{S_{a,K}} < P_{S_{s,K}}\right)$ refers to the lack possibility of the SPV units, and $E\left(P_{S_{a,K}} < P_{S_{s,K}}\right)$ denotes the predictable power of the SPV unit fewer than $P_{S_{s,K}}$.

E. CARBON TAX MODEL

The conventional units discharge emissions to the environment. During the production from thermal units rises, these gasses including SO_x and NO_x also increases. The dangerous emissions are described in (ton/hr) as below:

$$\begin{aligned} E = &\sum_{i=1}^{N_G}\left(a_i P_{cg,i}^2 + b_i P_{cg,i} + c_i\right)\times 0.01 \\ &+ \omega_i e^{\left(P_{cg,i}\mu_i\right)} \end{aligned} \tag{9}$$

where $a_i, b_i, c_i, \omega_i and \mu_i$ are the emission coefficients of the thermal units.

Lately, to protection the environment, generate clean energy, and address global warming hazards, numerous countries are obliging a carbon tax on harmful gases emissions. Furthermore, the power generation companies are target to huge pressure in order to produce unpolluted energy from RES and to decrease their harmful gases. CT is forced on these harmful gases model. The carbon emission cost ($/hr) can be represented as below:

$$C_{EC} = C_T \times E \tag{10}$$

where C_T is the gasses' carbon tax per unit value.

F. FITNESS FUNCTIONS

In OPF, mathematical models are used to find the optimal set points for generators and other controllable devices in the power system, enabling power system operators and planners to make informed decisions about the optimal dispatch of power units. The fitness functions of optimal power flow problem are stated consists of various models described in the preceding subsections. There are two considered fitness functions in this article as below:

1) DECREASING OF THE TOTAL COST

The initial fitness function in this study focuses on minimizing the total cost without considering emissions. In contrast, the second fitness function incorporates emissions as a factor. Therefore, the primary goal of the first fitness function is to minimize [18]:

$$\begin{aligned} F_1 = F\left(P_{cg}\right) + \sum_{j=1}^{N_W} \Big[& C_{W_j}\left(P_{W_{s,j}}\right) \\ & + C_{U_{w,j}}\left(P_{W_{a,j}} - P_{W_{s,j}}\right) \\ & + C_{O_{w,j}}\left(P_{W_{s,j}} - P_{W_{a,j}}\right)\Big] \\ & + \sum_{K=1}^{N_P} \Big[C_{S_k}\left(P_{S_{s,k}}\right) \\ & + C_{U_{S,K}}\left(P_{S_{a,K}} - P_{S_{s,K}}\right) \\ & + C_{O_{s,K}}\left(P_{S_{s,K}} - P_{S_{a,K}}\right)\Big] \end{aligned} \tag{11}$$

where N_W and N_P denote the total number of wind turbine and SPV generators, respectively. With taking into consideration the modeling of CT, the second fitness function is described by addition the CT from Eq.10 to the Eq.11.

$$\begin{aligned} F_2 = F\left(P_{cg}\right) + \sum_{j=1}^{N_W} \Big[& C_{W_j}\left(P_{W_{s,j}}\right) \\ & + C_{U_{w,j}}\left(P_{W_{a,j}} - P_{W_{s,j}}\right) \\ & + C_{O_{w,j}}\left(P_{W_{s,j}} - P_{W_{a,j}}\right)\Big] \\ & + \sum_{K=1}^{N_P} \Big[C_{S_k}\left(P_{S_{s,k}}\right) \\ & + C_{U_{s,K}}\left(P_{S_{a,K}} - P_{S_{s,K}}\right) \\ & + C_{o_{s,K}}\left(P_{S_{s,K}} - P_{S_{a,K}}\right)\Big] + C_{EC} \end{aligned} \tag{12}$$

Additionally, these two fitness functions are subjected to equality and inequality restrictions that are represented as follows.

2) THE ACTIVE TRANSMISSION LOSSES

The active transmission losses are described from the following equation [18]:

$$P_L = \sum_{k=1}^{n_l} G_k \left[V_i^2 + V_j^2 - 2V_iV_j cos\left(\theta_i - \theta_j\right)\right] \tag{13}$$

where P_L represents the real transmission loss, G_k denotes the conductance of k'th line, V_i, V_j, θ_i and θ_j represent the magnitudes of voltage and the angles at buses i and j, respectively.

3) THE VOLTAGE DEVIATIONS

The voltage deviations at load buses can be described as follows:

$$V_D = \sum_{j=1}^{N_L} |V_k - 1| \tag{14}$$

a nominal value represents 1 p.u. that can be used as a reference value.N_L refers to the buses' number for the load.

4) EQUALITY RESTRICTIONS

The equality limitations represent the load flow equations utilized to ensure power balance, which can be written from the following equation:

$$P_{Gi} - P_{Di} - V_i \sum_{j=1}^{N_L} V_j \left(G_{ij}\cos\theta_{ij} + B_{ij}\sin\theta_{ij}\right) = 0 \tag{15}$$

$$Q_{Gi} - Q_{Di} - V_i \sum_{j=1}^{N_L} V_j \left(G_{ij}\sin\theta_{ij} - B_{ij}\cos\theta_{ij}\right) = 0 \tag{16}$$

where P_{Gi} and Q_{Gi} represent the real and reactive power generated, respectively. P_{Di} represents demand active power of the bus j while Q_{Di} denote demand reactive power of the bus j. G_{ij} refers to the transfer conductance between 2 buses while B_{ij} represents the susceptance between 2 buses.

5) INEQUALITY RESTRICTIONS

The inequality limitations define operational bounds for elements within the power network, encompassing security restrictions associated load buses and transmission lines.

6) UNIT RESTRICTIONS

Voltage levels and real power outputs at all generator buses must be restricted to fall within their specified lower and upper limits:

$$V_{Gi}^{min} \leq V_{Gi} \leq V_{Gi}^{max}, \quad i = 1, 2, 3 \ldots, N_T \tag{17}$$

$$P_{cg,i}^{min} \leq P_{cg,i} \leq P_{cg,i}^{max}, \quad i = 1, 2, 3 \ldots, N_g \tag{18}$$

$$P_{W_{s,j}}^{min} \leq P_{W_{s,j}} \leq P_{W_{s,j}}^{max}, \quad j = 1, 2, 3 \ldots, N_W \tag{19}$$

$$P_{S_{s,K}}^{min} \leq P_{S_{s,K}} \leq P_{S_{s,K}}^{max}, \quad k = 1, 2, 3 \ldots, N_P \tag{20}$$

$$Q_{cg,i}^{min} \leq Q_{cg,i} \leq Q_{cg,i}^{max}, \quad i = 1, 2, 3 \ldots, N_g \tag{21}$$

$$Q_{W_{s,j}}^{min} \leq Q_{W_{s,j}} \leq Q_{W_{s,j}}^{max}, \quad j = 1, 2, 3 \ldots, N_W \tag{22}$$

$$Q_{S_{s,K}}^{min} \leq Q_{S_{s,K}} \leq Q_{S_{s,K}}^{max}, \quad k = 1, 2, 3 \ldots, N_P \tag{23}$$

where N_T is the number of unit buses. Equation 17 is the voltage bounds of the unit buses. Eqs. 18−20 are the real power bounds for the thermal generators, WT and SPV units. Eqs. 21−23 are the reactive power capabilities for wholly generating buses.

7) LINE AND LOAD BUS VOLTAGES' CONSTRAINTS

$$S_{li} \leq S_{li}^{max}, \quad i = 1, 2, 3 \ldots, N_l \tag{24}$$

$$V_{Li}^{min} \leq V_{Li} \leq V_{Li}^{max}, \quad i = 1, 2, 3 \ldots, N_L \tag{25}$$

where S_{li} is the apparent power of the line i'th. S_{li}^{max} denotes the maximum boundary of the apparent power of line i'th. V_{Li}^{min}, V_{Li}^{max} refer to the lower and upper voltage magnitude, respectively. N_l is the transmission lines' number.

III. THE STOCHASTIC WT AND SPV POWER MODELS

To model the mean power output of the wind turbine units, Weibull probability density functions (PDFs) are utilized in the following equation:

$$f_v(v) = \frac{K}{C}.(\frac{v}{C})^{K-1}.e^{-(\frac{v}{C})^K} \tag{26}$$

where v refers to the wind speed m/s, K denotes Weibull distribution shape parameter, while C represents the Weibull distribution scale parameter.

The mean of Weibull distribution is represented as follows,

$$M_{wt} = C.\Gamma(1 + {}^1/_K) \tag{27}$$

The gamma function is calculated as:

$$\Gamma x = \int_0^\infty t^{x-1} e^{-t} dt, \quad x > 0 \tag{28}$$

The WT units output basically is influenced by the speed of wind and WT's power curve and can be described from this equation:

$$P_w(v) = \begin{cases} 0 & v \leq v_{ci} \& v > v_{co} \\ \dfrac{v^2 - v_{ci}^2}{v_{nom}^2 - v_{ci}^2}.P_{W_r} & v_{ci} < v \leq v_{nom} \\ P_{W_r} & v_{nom} < v \leq v_{co} \end{cases} \tag{29}$$

where v_{ci}, v_{co}, and v_{nom} denote the cut-in, cut-out and rated wind speed, respectively. Whilst P_{W_r} represent the rated power from the WT units. As observed from Equation 29, when v surpasses v_{co} but remains below v_{ci}, the output power becomes zero. Additionally, the wind turbine (WT) generates power as soon as the wind speed falls between v_{nom} and v_{co}. The probabilities associated with these discrete regions can be expressed as follows [36]:

In contradiction of the stated discrete regions, the WT

$$F_w(P_w)\{P_w = 0\} = 1 - \exp\left(-\left(\frac{v_{ci}}{c}\right)^k\right) + \exp\left(-\left(\frac{v_{co}}{c}\right)^k\right) \tag{30}$$

$$F_w(P_w)\{P_w = P_{wr}\} = \exp\left(-\left(\frac{v_{nom}}{c}\right)^k\right) - \exp\left(-\left(\frac{v_{co}}{c}\right)^k\right) \tag{31}$$

output power is continuous between cut in and rated wind speeds. Thus, possibility for this area is given from the following equation [36]:

$$F_w(P_w) = \frac{K(v_{nom} - v_{ci})}{C^K * P_{wr}} \left(v_{ci} + \frac{P_w}{P_{wr}}(v_{nom} - v_{ci})\right)^{k-1} * \exp\left(-\left(\frac{v_{ci} + \frac{P_w}{P_{wr}}(v_{nom} - v_{ci})}{c}\right)^k\right) \tag{32}$$

Likewise, to accommodate a broader range of weather conditions, the lognormal function is employed to provide a more precise description of the frequency distribution. The mean and standard deviation (STD) values of the global irradiation is employed for deriving the parameters of the lognormal distribution function. The output power of Solar Photovoltaic units is correlated with solar irradiance (I), which follows a lognormal probability distribution function (PDF). The probability distribution of solar irradiance can be stated using the following equation:

$$f_I(I) = \frac{I}{I\boldsymbol{\mu}\sqrt{2\pi}}.e^{\left(\frac{-[lnX-\sigma]^2}{2\mu}\right)}, \quad I > 0 \tag{33}$$

where μ is the mean while σ denote the STD. The lognormal distribution mean can be represented from the following equation:

$$M_{ld} = e^{(\sigma + \frac{\mu^2}{2})} \tag{34}$$

The direct correlation between irradiance of the solar and the SPV units' energy can be expressed from the following equation [37].

$$P_{sr}(I) = \begin{cases} P_{sr}\left(\dfrac{I^2}{I_{sr}I_c}\right); & 0 < I < I_c \\ P_{sr}\left(\dfrac{I}{I_{sr}}\right); & I > I_c \end{cases} \tag{35}$$

where P_{sr} refers to the rated output of the SPV units, I_c represents a definite irradiance point, and I_{sr} denotes the solar irradiance at rated environment. It's worth highlighting that the scheduled energy for solar power is not fixed; instead, it represents a mutually agreed-upon power level between system operators and the private entity selling solar power. The computing of underestimation and overestimation costs

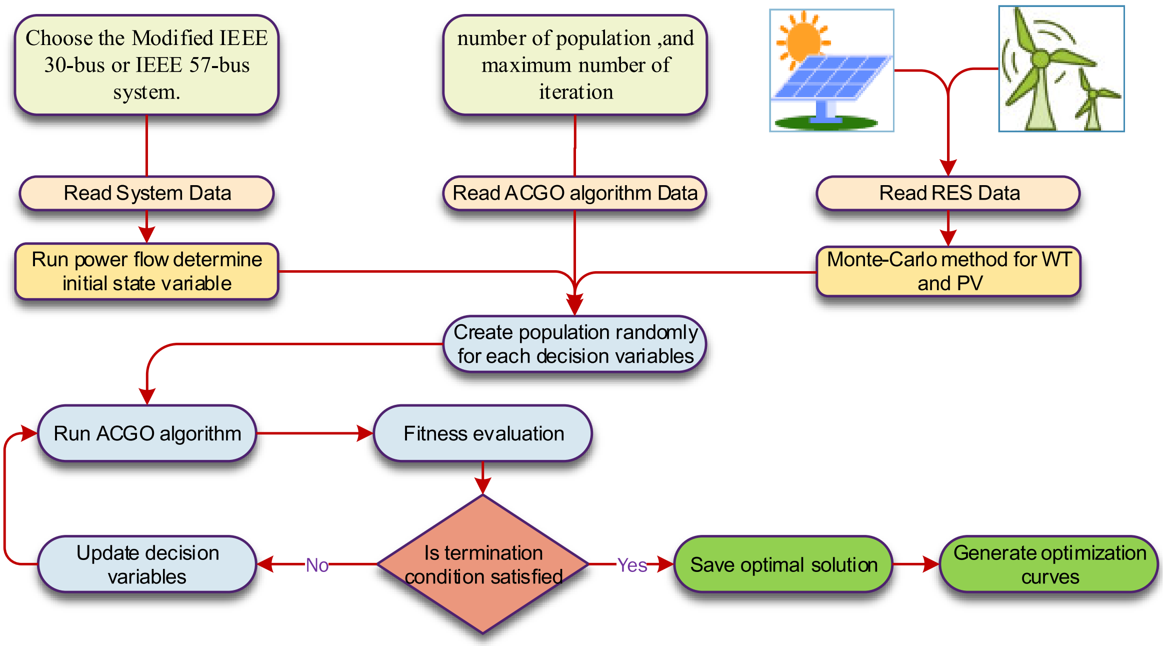

FIGURE 1. The flowchart of ACGO for the OPF problem.

for Solar Photovoltaic (SPV) units can be determined as follows [38]:

$$C_{U_S}\left(P_{S_a}-P_{S_s}\right)=p_S\left(P_{S_a}-P_{S_s}\right)=p_S\sum_{N=1}^{N+}\left[P_{S_{S+}}-P_{S_S}\right]*f_{ps+} \quad (36)$$

$$C_{O_S}\left(P_{S_s}-P_{S_a}\right)=R_S\left(P_{S_s}-P_{S_a}\right)=R_S\sum_{N=1}^{N-}\left[P_{S_S}-P_{S_{S-}}\right]*f_{ps-} \quad (37)$$

where $P_{S_{S+}}$ and $P_{S_{S-}}$ refer to the surplus power and shortage power.f_{ps+} and f_{ps-} represent the relative frequencies for the happening of $P_{S_{S+}}$ and $P_{S_{S-}}$.

Figure 1 showcases the flowchart of the proposed ACGO technique for optimizing the OPF problem with renewable energy sources. The flowchart visually represents the detailed steps involved in the OPF process using the ACGO method. It presents a sequential series of operations that outline how the OPF, incorporating RES, is solved by the ACGO technique to attain an optimal solution within a power system.

IV. MATHEMATICAL MODEL OF THE METAHEURISTIC ALGORITHMS

Hybrid metaheuristic algorithms are a powerful class of optimization techniques that combine elements of multiple metaheuristics to enhance their performance and problem-solving capabilities. These algorithms are designed to tackle complex optimization problems, where traditional optimization methods may struggle to find satisfactory solutions. The mathematical models underlying hybrid metaheuristic algorithms integrate the strengths of different search strategies in order to exploit their synergies and overcome their individual limitations. In this paper, it was suggested hybrid metaheuristic optimization algorithm between the CGO algorithm and AEO algorithm. By fusing these techniques, hybrid metaheuristic algorithms aim to strike a balance between exploration and exploitation. This section outlines the original procedure of the CGO and AEO techniques.

A. CHAOS GAME OPTIMIZATION

This process adheres to specific guidelines derived from the chaos concept, employing a fractal approach inspired via the chaos game concept. Initially, an initialization process is executed using establishing the initial locations of the candidate solutions as follows [21]:

$$X=\begin{bmatrix}X_1\\X_2\\\cdot\\\cdot\\X_i\\\cdot\\\cdot\\X_n\end{bmatrix}=\begin{bmatrix}x_1^1x_1^2\ldots\ldots x_1^j\ldots\ldots x_1^d\\x_2^1x_2^2\ldots\ldots x_2^j\ldots\ldots x_2^d\\\ldots\\\ldots\\x_i^1x_i^2\ldots\ldots x_i^j\ldots\ldots x_i^d\\\ldots\\\ldots\\x_n^1x_n^2\ldots\ldots x_n^j\ldots\ldots x_n^d\end{bmatrix},\begin{cases}i=1,2,\ldots.,m\\j=1,2,\ldots..,d\end{cases} \quad (38)$$

$$x_i^j(0) = x_{i,min}^j + rand.\left(x_{i,max}^j - x_{i,min}^j\right), \begin{cases} i = 1, 2, \ldots, m \\ j = 1, 2, \ldots, d \end{cases} \tag{39}$$

where d is the problem's dimension and m represents the total number of initialized candidates within the problem space. $x_{i,min}^j$, $x_{i,max}^j$ are the lower and upper limits of the decision variables. The mathematical representation of the $seed_i^1$ is as follows [21]:

$$seed_i^1 = X_i + \alpha_i \times (\beta_i - GB - \gamma_i \times MG_i), \quad i = 1, 2, \ldots, m \tag{40}$$

where GB denotes the global optimum, α_i is the movement constraint factor, and β_i and γ_i are vectors randomly formed by numbers in the range of [1,0]. MG_i represents the mean group. $seed_i^2$ can be calculated as follows [21]:

$$seed_i^2 = GB + \alpha_i \times (\beta_i \times X_i - \gamma_i \times MG_i), \quad i = 1, 2, \ldots, m \tag{41}$$

While $seed_i^3$ is mathematically computed as below [21]:

$$seed_i^3 = MG_i + \alpha_i \times (\beta_i \times X_i - \gamma_i \times GB), \quad i = 1, 2, \ldots, m \tag{42}$$

Finally, $seed_i^4$ is mathematically calculated as follows [21]:

$$seed_i^4 = X_i\left(x_i^k = x_i^k + R\right), k = [1, 2, \ldots, d] \tag{43}$$

where R is randomly formed by numbers in the range of [1,0].

B. ARTIFICIAL ECOSYSTEM-BASED OPTIMIZATION

The original AEO technique was presented by Zhao et al which is according to the concept of the energy flow within a natural ecosystem [20]. This algorithm has three types of behaviors included production, consumption, and decomposition The conventional AEO technique including three operators [39];

- Production serves the determination of maintaining the balance between the exploration and exploitation stages,
- The consumption plays a role in an enhancement of exploration,
- The decomposition operator is utilized to improve the exploitation aspect of the original AEO technique.

1) PRODUCTION

The production operator is modeled as below [40]:

$$x_1(t+1) = (1-a)\, x_n(t) + a \times x_{rand}(t) \tag{44}$$

$$a = (1 - \frac{t}{\max\_it})r_1 \tag{45}$$

$$x_{rand} = r(u_b - l_b) + l_b \tag{46}$$

where, a denotes a linear weight coefficient, while x_{rand} refers to a randomly generated individual location within the search space, and max_it denotes the maximum number of iterations, r_1 is a random number that is in the range [1,0]. r refers to the random vector inside the range of [1,0], and u_b and l_b are the upper and lower bounds, respectively.

2) THE CONSUMPTION

There are of three types of consumers as the following equations:

a) herbivore is mathematically formulated as follows:

$$x_i(t+1) = x_i(t) + C \times (x_i(t) - x_1(t)), \quad i \in [2, \ldots, n] \tag{47}$$

$$C = \frac{1}{2}\frac{v_1}{|v_2|} \tag{48}$$

$$v_1 \sim N(0,1), v_2 \sim N(0,1), \tag{49}$$

where, N (0, 1) denotes a normal distribution.

b) carnivore is presented mathematically as below:

$$\begin{cases} x_i(t+1) = x_i(t) + C \times \left(x_i(t) - x_j(t)\right), \\ i \in [2, \ldots c., n] \\ j = randi([2i-1]) \end{cases} \tag{50}$$

c) omnivore can be modeled and calculated mathematically from the following equation:

$$\begin{cases} x_i(t+1) = x_i(t) + C \times (x_i(t) - x_1(t)) \\ \qquad + (1 - r_2) \\ \left(x_i(t) - x_j(t)\right), i = 3, \ldots c., n \\ j = randi([2i-1]) \end{cases} \tag{51}$$

3) DECOMPOSITION

The decomposition operator is modeled mathematically as follows:

$$x_i(t+1) = x_n(t) + D \times \left(s \times x_n(t) - q \times x_i(t)\right), \quad i = 1, \ldots, n \tag{52}$$

$$D = 3u, \quad uN(0,1) \tag{53}$$

$$s = r_3 \times randi([12]) - 1 \tag{54}$$

$$q = 2 \times r_3 - 1 \tag{55}$$

where, the D denotes the decomposition factor D, while s and q represent the weight coefficients. The flow chart of the ACGO technique is displayed in Figure 2. The hybrid ACGO algorithm offers several advantages over the original AEO and CGO techniques:

Advantages of ACGO:

1) Improved Exploration Capability: ACGO enhances the exploration capability compared to AEO and CGO algorithms. This means that it is better at searching through the solution space to find potentially better solutions. It can explore a wider range of possibilities,

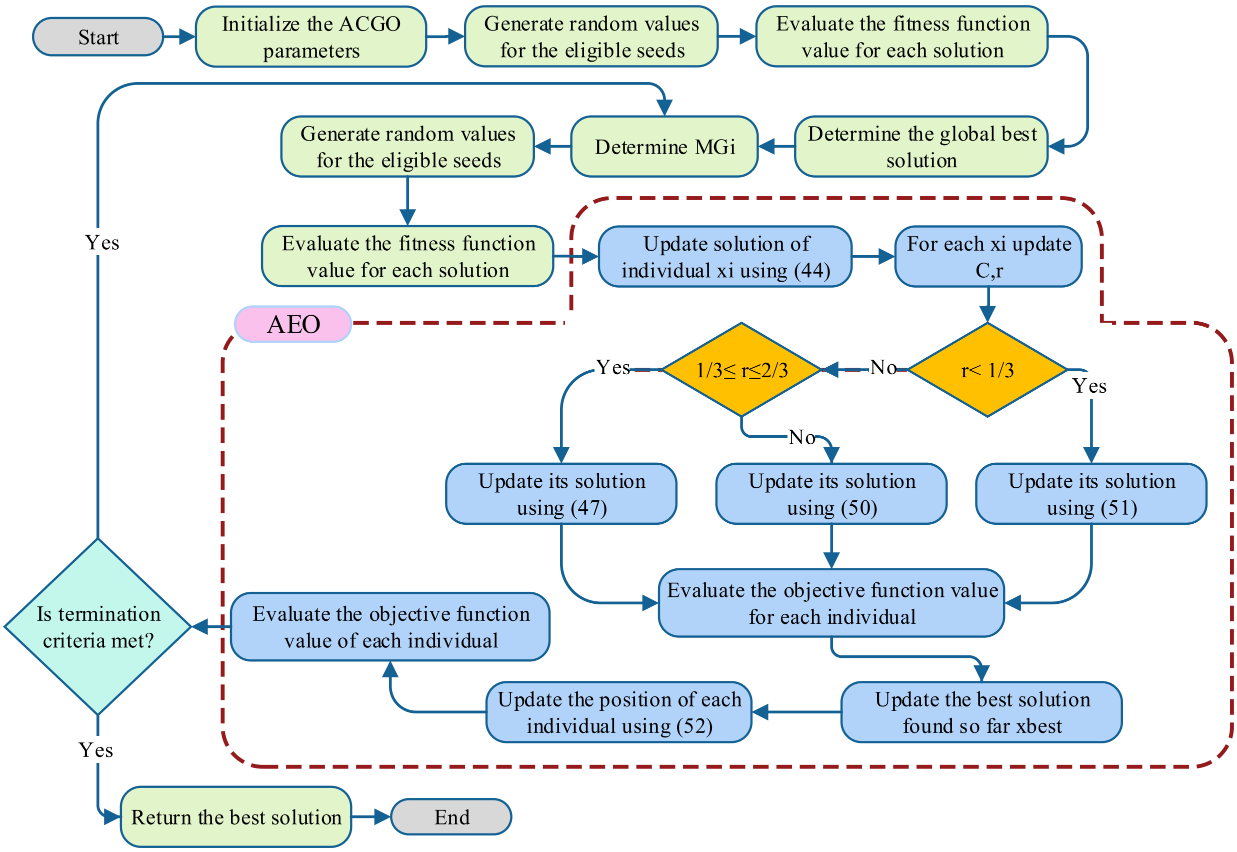

FIGURE 2. **The flowchart of the hybrid ACGO technique.**

which is crucial for solving complex optimization problems like the OPF problem with RES.

2) Avoidance of Local Minima: A significant advantage of ACGO is that its exploration ability does not diminish based on the number of iterations. This is a critical feature as it helps the algorithm to avoid getting trapped at local minima solutions. Local minima are suboptimal solutions that can mislead optimization algorithms into converging prematurely. By maintaining strong exploration throughout the optimization process, ACGO is better equipped to find globally optimal or near-optimal solutions.

However, like any algorithm, ACGO may have its own shortcomings. One potential disadvantage of the hybrid ACGO algorithm could be:

Integrating different optimization techniques and maintaining robust exploration capabilities can increase the computational burden. Therefore, ACGO may not be suitable for problems with where quick results are needed.

V. SIMULATION RESULTS AND DISCUSSION

In this section, the outcomes of the trials performed on seven standard test functions utilizing the proposed optimizer and contemporary algorithms are exhibited. The experiments offer a thorough assessment of the methods from diverse angles, such as exploration and exploitation capabilities and convergence. Furthermore, the section comprises four instances that evaluate the efficiency and appropriateness of the ACGO algorithm that has been introduced.

A. BENCHMARK FUNCTIONS

In this subsection, we illustrate the effectiveness of the ACGO technique through evaluations on seven benchmark functions. The mathematical expressions for those test functions are detailed in Table 1. The experiments for these benchmarks are conducted by MATLAB (R2016a) on a computer equipped with an Intel(R) Core i5-4210U CPU running at 2.40 GHz and 8GB of RAM. This study employs seven widely recognized benchmark test functions to assess and compare the ACGO technique's performance. For all the metaheuristic methods discussed in this paper, a uniform maximum iteration limit of 200 iterations is adopted, accompanied by a consistent population size of 50. In this subsection, the ACGO technique is compared with five recently proposed techniques such as: GBO [41], INFO [42], NGO [43], AEO, and CGO algorithms.

This study establishes the predominance of the achieved solution through the utilization of mean value and standard deviation. The algorithm demonstrating lower mean

TABLE 1. Benchmark functions.

Name	Function	Dim	Range	f_{min}
Sphere	$F_1(x) = \sum_{i=1}^{N} x_i^2$	30	[-100,100]	0
Schwefel 2.22	$F_2(x) = \sum_{i=1}^{N} \lvert x_i \rvert + \prod_{i=1}^{N} \lvert x_i \rvert$	30	[-10,10]	0
Schwefel 1.2	$F_3(x) = \sum_{i=1}^{N} \left(\sum_{j-1}^{i} x_j \right)^2$	30	[-100,100]	0
Schwefel 2.21	$F_4(x) = max_i\{\lvert x_i \rvert, 1 \leq i \leq N\}$	30	[-100,100]	0
Rosenbrock	$F_5(x) = \sum_{i=1}^{N-1} [100(x_{i+1} - x_i^2)^2 + (x_i - 1)^2$	30	[-30,30]	0
Step	$F_6(x) = \sum_{i=1}^{N} (\lvert x_i + 0.5 \rvert)^2$	30	[-100,100]	0
Quartic	$F_7(x) = \sum_{i=1}^{N} ix_i^4 + random[0,1]$	30	[-1.28,1.28]	0

value and standard deviation emerges as possessing robust capabilities for global optimization and greater stability. The statistical outcomes obtained from the ACGO algorithm and five widely recognized algorithms, employed to solve seven benchmark functions, are showcased in Table 2. According to the information in the table, the ACGO technique outperforms other assessed methodologies across the majority of benchmark functions in relation to mean value. The data indicates that the ACGO algorithm consistently obtains more favorable solutions compared to recently proposed techniques for solving various benchmark functions. Furthermore, it is evident that the ACGO approach surpasses GBO, INFO, NGO, AEO, and CGO techniques in addressing benchmark functions. This analysis underscores the efficiency of the ACGO algorithm.

The tied rank method is a statistical approach employed to compare the performance of several techniques when the performance metric has ties, meaning that there are two or more observations that have the same value. Once the ranks have been assigned, the ranks for each algorithm are summed and compared. The algorithm with the lowest rank sum is considered to have performed better than the others. The data presented in Table 2 clearly indicates that the ACGO technique exhibits superior performance across the majority of the 7 benchmark optimization problems, as evidenced by its ranking order. Following closely in second and third positions are the CGO and AEO algorithms, both of which demonstrate robust efficacy. This collective evidence demonstrates that the ACGO technique stands out as a highly effective algorithm for successfully identifying optimal solutions within this category of problems.

Furthermore, the convergence curves indicate that the ACGO technique consistently exhibits superior performance compared to the other techniques across most of these benchmark functions, demonstrating its robustness and versatility in handling a varied range of optimization problems. The superior performance of the ACGO technique is attributed to its effective combination of the AEO algorithm and CGO technique, which enables it to competently explore the search space and exploit promising regions, leading to faster convergence and better solutions. In addition, the convergence curves reveal that the original GBO, INFO, NGO, AEO, and CGO techniques exhibit slower convergence rates and may get stuck in local optima. The convergence curves in Figure 3 demonstrate that the ACGO technique not only achieves fast convergence but also maintains stable and consistent performance throughout the optimization process. This is an important characteristic of an optimization algorithm since it confirms that the technique can reliably find the optimum solution without being stuck in local minima. Moreover, the experimental results suggest that the ACGO technique is robust to the choice of optimization parameters, such as population size and crossover probability. This indicates that the ACGO algorithm can be easily adapted to different problem domains without requiring extensive parameter tuning. Overall, the results prove that the ACGO technique is a powerful and versatile optimization technique that is effectively utilized to attain the optimal solution for

TABLE 2. The statistical results of seven benchmark functions by the ACGO algorithm and other well-known techniques.

Function		ACGO	AEO	CGO	GBO	INFO	NGO
F1	Best	1.5E-139	1.05E-79	2.8E-58	9.06E-52	4.44E-49	5.01E-34
	Average	9.5E-125	3.75E-69	1.15E-55	4.1E-46	1.84E-43	7.16E-33
	Median	1.5E-130	1.03E-73	2.82E-56	1.73E-49	9.67E-46	4.24E-33
	Worst	1.9E-123	7.48E-68	9.58E-55	4.79E-45	2.45E-42	3.02E-32
	std	4.2E-124	1.67E-68	2.48E-55	1.27E-45	5.79E-43	8.77E-33
	Rank	1	2	3	4	5	6
F2	Best	1.11E-75	2.43E-41	2.97E-30	2.03E-28	1.08E-24	6.6E-18
	Average	6.27E-63	1.52E-36	5.02E-29	1.95E-24	1.83E-22	1.65E-17
	Median	1.86E-65	1.09E-38	2.13E-29	1.77E-25	1.11E-23	1.58E-17
	Worst	5.29E-62	1.59E-35	2.96E-28	1.95E-23	3.2E-21	3.85E-17
	std	1.62E-62	3.8E-36	7.04E-29	4.64E-24	7.11E-22	7.66E-18
	Rank	1	2	3	4	5	6
F3	Best	1.2E-124	5.75E-78	1.93E-40	3.42E-42	1.16E-39	1.04E-08
	Average	5.4E-114	2.26E-64	2.18E-37	2.56E-38	1.27E-32	1.19E-06
	Median	2.9E-118	4.1E-72	1.64E-38	5.51E-40	4.71E-35	1.85E-07
	Worst	1E-112	4.35E-63	2.41E-36	2.05E-37	1.65E-31	1.35E-05
	std	2.3E-113	9.71E-64	5.61E-37	5.68E-38	3.71E-32	3.02E-06
	Rank	1	2	4	3	5	6
F4	Best	8.27E-67	8.95E-41	2.76E-25	1.54E-24	1.21E-22	1.39E-14
	Average	1.56E-59	2.29E-33	3.64E-23	8.59E-22	8.95E-19	3.71E-14
	Median	1.16E-62	2.58E-37	1.72E-23	1.22E-22	1.88E-20	3.34E-14
	Worst	1.53E-58	4.24E-32	1.59E-22	1.08E-20	1.5E-17	7.08E-14
	std	4.48E-59	9.47E-33	4.89E-23	2.47E-21	3.34E-18	1.77E-14
	Rank	1	2	3	4	5	6
F5	Best	14.6599	24.5311	17.88338	24.25387	23.12486	26.83203
	Average	18.3316	25.58646	19.75382	25.13063	24.43097	27.31122
	Median	18.3877	25.71687	20.1513	25.117	24.41788	27.2574
	Worst	21.256	26.62456	21.53792	26.10917	25.78378	27.8186
	std	1.458657	0.540684	1.096515	0.565603	0.620893	0.253381
	Rank	1	5	2	4	3	6
F6	Best	2.61E-16	0.000837	3.65E-14	0.00018	1.16E-06	0.189623
	Average	2.02E-13	0.005177	7.31E-12	0.00108	1.47E-05	0.337336
	Median	2.8E-14	0.005165	1.81E-12	0.000875	8.52E-06	0.314621

TABLE 2. *(Continued.)* **The statistical results of seven benchmark functions by the ACGO algorithm and other well-known techniques.**

	Worst	1.31E-12	0.010039	8.59E-11	0.002836	3.81E-05	0.557148
	std	3.81E-13	0.002406	1.89E-11	0.000702	1.31E-05	0.115208
	Rank	1	5	2	4	3	6
F7	Best	0.000129	0.000246	9.88E-05	0.000111	0.000201	0.000308
	Average	0.000428	0.001021	0.000674	0.001192	0.00178	0.001318
	Median	0.000349	0.000938	0.000627	0.000985	0.00135	0.001333
	Worst	0.000861	0.003499	0.001832	0.004017	0.005593	0.003044
	std	0.00023	0.000763	0.000456	0.001008	0.001428	0.000676
	Rank	1	3	2	4	6	5
Average Rank		1	3	2.714286	3.857143	4.571429	5.857143
Final ranking		1	3	2	4	5	6

a widespread range of real-world optimization problems. The fast convergence, stable performance, and robustness to parameter settings make the ACGO algorithm an attractive choice for practitioners and researchers alike. The numerical data is depicted in box plots, illustrating the diverse optimal values achieved across various runs corresponding to a specific algorithm. Figure 4 displays the box plots for seven benchmark functions, utilizing data gathered from the algorithms over 30 individual iterations. Box plots excel at representing data distribution, making them excellent tools to underscore data agreement. Upon examining Figure 4, it becomes evident that the box plots for the proposed ACGO technique exhibit narrow spreads and rank among the lowest values across most functions. These visual representations serve as effective tools for assessing the performance of the nonlinear system, offering a clear juxtaposition of various techniques. The results underscore that the ACGO method outperforms its counterparts.

1) WILCOXON'S RANK TEST RESULTS

In this subsection, the variances between ACGO and other techniques are additional analyzed statistically using the Wilcoxon rank-sum test (WRST), which is a paired assessment is employed to notice significant differences between the two techniques. The obtained results of the test between ACGO and each technique, conducted at a significance level of α =0.05 are presented in Table 3, where the symbols "+/=/-" show whether ACGO executes better, similarly, or worse than the compared technique. Additionally, the table includes statistical findings for ACGO across different dimensions and functions, indicating whether ACGO performs better, similarly, or worse than the comparison algorithm. ACGO demonstrates superior statistical performance in F1-F7 with Dim=30 when compared to other techniques, affirming its significant dominance across most functions. Consequently, it is confidently concluded that the proposed ACGO technique exhibits the best overall performance when compared to other methods.

2) FRIEDMAN'S RANK TEST RESULTS

Table 4 shows the statistical results achieved using Friedman tests [44] for seven benchmark functions using the studied algorithms. A lower ranking value indicates superior algorithm performance. According to the results, the ranking order of the six techniques is as follows: ACGO, CGO, AEO, GBO, INFO, and NGO.

Furthermore, Figure 5 presents the mean ranks obtained from Friedman's rank test for the seven benchmark functions using various algorithms. This visualization provides a clear comparison of the algorithms' performances across the cases, helping to identify any significant differences in their ranks. The top-ranking position clearly indicates that ACGO is the most effective algorithm among the six considered.

B. THE STUDY CASE RESULTS

In this subsection, the competence of the ACGO method is presented using the modified IEEE-30 bus test system. The simulation results of the ACGO technique which are compared with that attained using the original AEO and CGO for the modified IEEE-30 bus test and the modified IEEE-57 bus test system. The target of the ACGO technique is to reduce both the total generation cost and improve convergence speed. eight scenarios are assessed including various kinds of RES. The use of original AEO, CGO and the proposed ACGO algorithms to OPF problem with and without RES have been executed on laptop. The

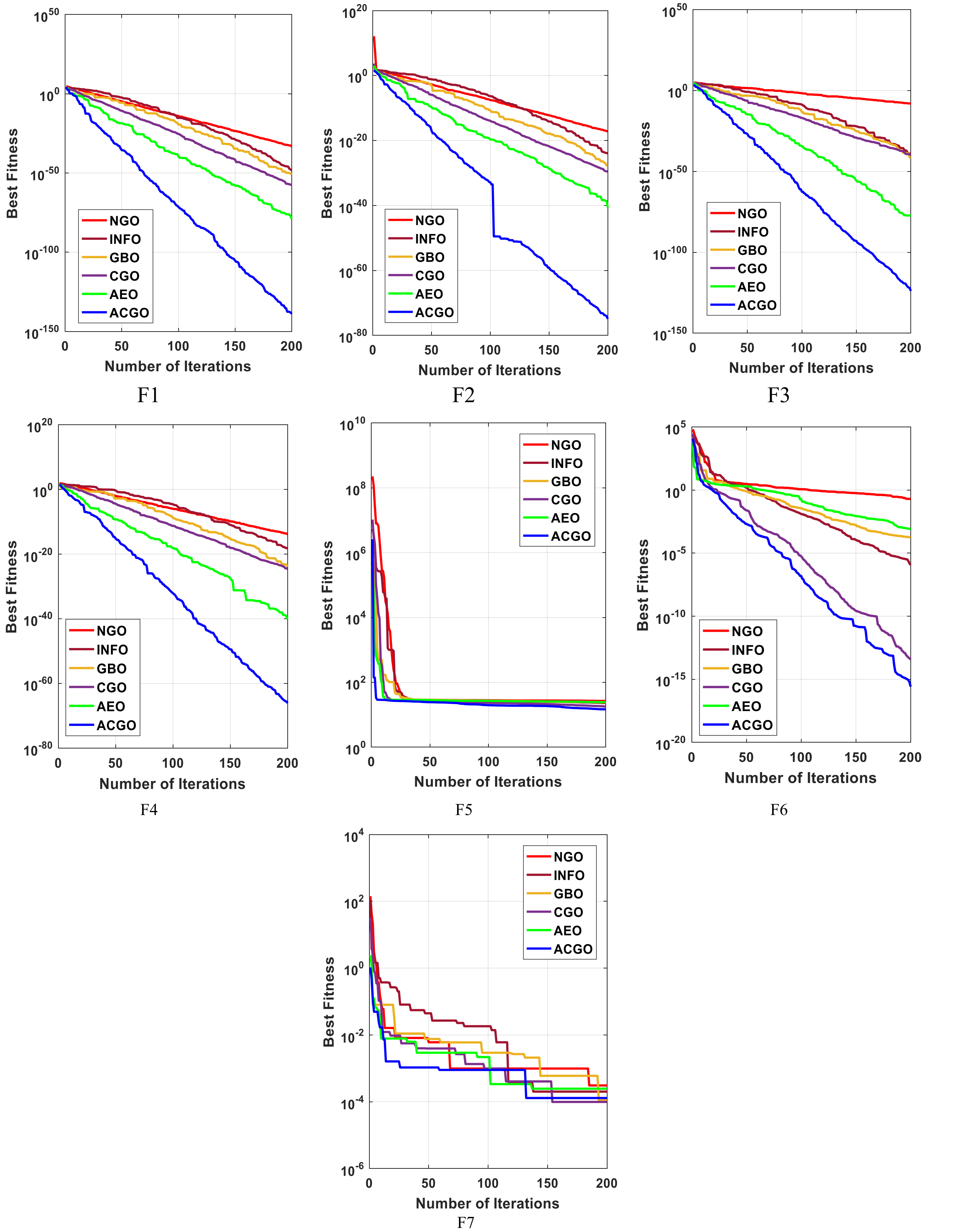

FIGURE 3. The convergence characteristics of the studied techniques for the benchmark functions.

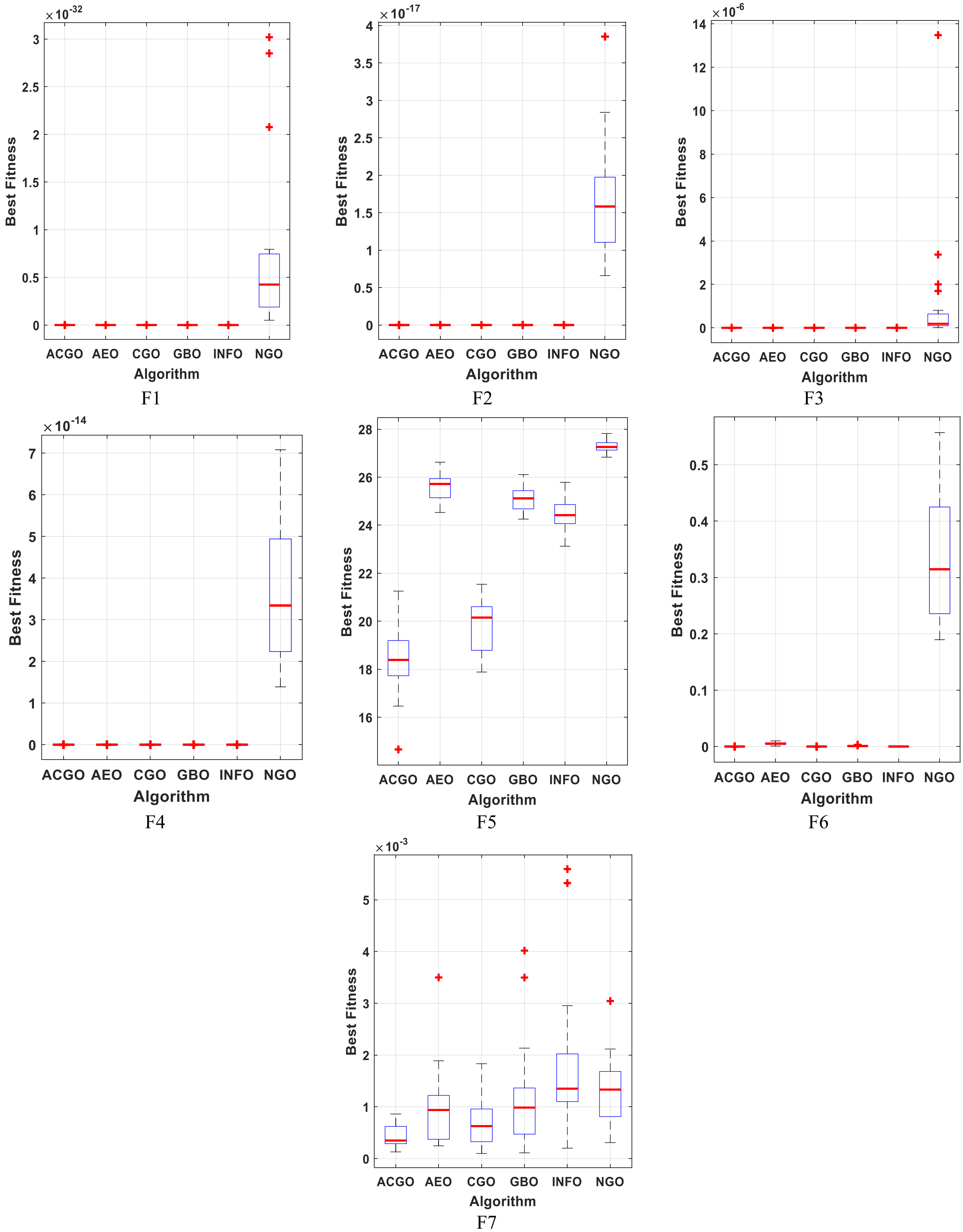

FIGURE 4. **Boxplots of the studied techniques for the benchmark functions.**

TABLE 3. Statistical results of the Wilcoxon rank-sum test.

ACGO vs	AEO		CGO		GBO		INFO		NGO	
Function	P	winner	P	winner	P	winner	P	winner	P	winner
F1	6.796E-08	+	6.796E-08	+	6.796E-08	+	6.796E-08	+	6.796E-08	+
F2	6.786E-08	+	6.786E-08	+	6.786E-08	+	6.786E-08	+	6.786E-08	+
F3	6.796E-08	+	6.796E-08	+	6.796E-08	+	6.796E-08	+	6.796E-08	+
F4	6.796E-08	+	6.786E-08	+	6.796E-08	+	6.796E-08	+	6.796E-08	+
F5	6.796E-08	+	1.349E-03	+	6.796E-08	+	6.796E-08	+	6.796E-08	+
F6	6.796E-08	+	3.987E-06	+	6.796E-08	+	6.796E-08	+	6.796E-08	+
F7	1.349E-03	+	7.205E-02	=	7.579E-04	+	1.807E-05	+	9.748E-06	+
WRST (+/=/-)	7/0/0		6/1/0		7/0/0		7/0/0		7/0/0	

TABLE 4. Friedman test for the six algorithms.

Function	ACGO	AEO	CGO	GBO	INFO	NGO
F1	1	2	3	4.1	4.9	6
F2	1	2	3	4.1	4.9	6
F3	1	2	3.85	3.25	4.9	6
F4	1	2	3.35	3.75	4.9	6
F5	1.2	4.7	1.8	4.2	3.1	6
F6	1.05	4.9	1.95	4.1	3	6
F7	2	3.7	2.75	3.75	4.45	4.35
Mean ranks	1.178571	3.042857	2.814286	3.892857	4.307143	5.764286

specifications of the system are presented in Table 5. The number of iterations for each technique was determined as 100 for the modified IEEE-30 bus test system and it was determined as 200 for the modified IEEE-57 bus test system. Also, in order to confirm the consequence of the algorithms, all algorithms were run 20 times for the studied cases.

TABLE 5. Running platform specifications.

Name	Value
Hardware	
CPU	Core i5
Frequency	2.8GHz
RAM	16 GB
Software	
Operating system	Windows 10
Language	MATLAB 2016a

1) THE MODIFIED IEEE-30 BUS TEST SYSTEM.

The IEEE 30-bus system has 6 generators and twenty-four load buses. Moreover, there are forty-one branches which connection the generation units and load busses. Bus 1 was chosen to be the slack bus. The magnitude bounds of the voltage for the generators and load busses limits between 0.95 p.u. and 1.1 p.u. The setting of the tap changing transformers is changed from 0.9 p.u. to 1.1 p.u. Additionally, the VAR compensators are varied between 0 and 0.05 p.u. [35]. This system was modified in this article as defined in [35] to incorporate wind turbine and SPV units to the thermal units as shown in Table 6. The thermal generators are located at buses one, two and eight. Though, there are a SPV unit that is placed at bus 13 while there are 2 WT units are positioned at bus 5 and 11 [18].

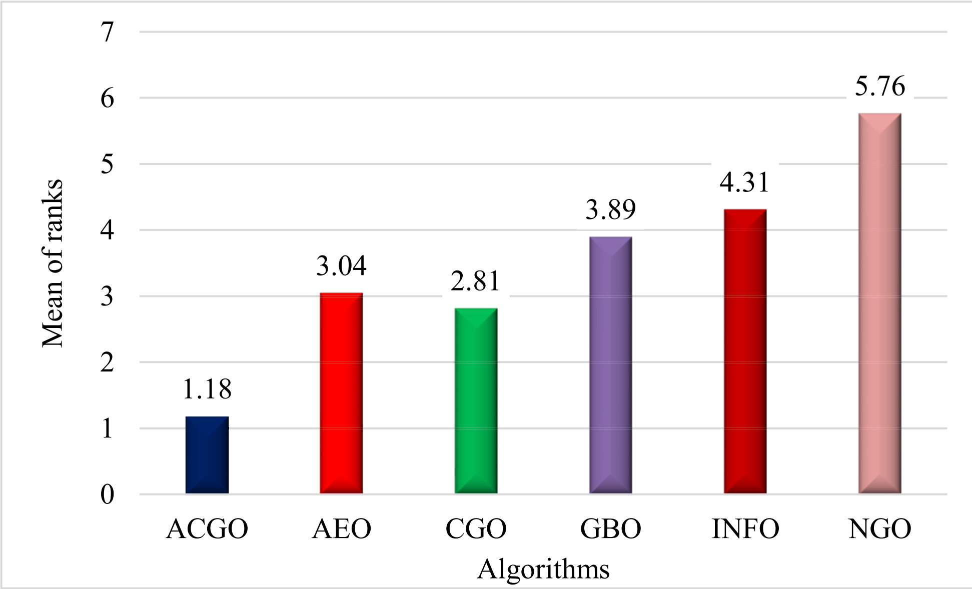

FIGURE 5. Mean ranks achieved using Friedman's rank test for the seven benchmark functions using various algorithms.

TABLE 6. Analysis of the modified IEEE-30 bus system.

Item	Quantity	Details
No. of buses	30	[35]
No. of	41	[35]
Thermal	3	Buses; 1 (Slack), 2, and 8
Wind	2	Buses; 5 and 11
Solar PV	1	Bus 13
Tap changing	4	At branch (6-9, 6-10, 4-12 and
Control variables	5	Scheduled actual power for 5 generators, including: Thg2, Thg3, WT1, WT2 and PV1
	6	The bus voltage of all
Connected	-	283.4 MW, 126.2 MVAr
Load bus	24	[0.95 – 1.05] p.u.
Generator	6	[0.95 – 1.1] p.u.

Figures 6a and 6b are presented the wind frequency distribution using Weibull fitting [13]. After running 8000 Monte-Carlo scenarios, the power curve was obtained. The Weibull PDF parameters for the WT unit at bus 5 are c = 9 and k = 2, and at bus 11 they are c = 10 and k = 2. The mean for the Weibull distribution is M_{wt} = 7.976 for bus 5 while M_{wt} = 8.862 m/s for bus 11. The rated power of each turbine is 3 MW and it was used with cut-in wind speed v_{ci}= 3 m/s, cut-out wind speed v_{co}= 25m/s and rated wind speed v_{nom}= 16m/s.

In the similar way to define the output of PV generators, the lognormal PDF parameters are selected according to the mean and STD of the global irradiation as in [45]. The σ= 6,μ= 0.6 while lognormal mean is I=483 W/m. Afterward executing the Monte-Carlo method with a sample size of 8000, the frequency distribution along with solar irradiance's lognormal fitting is displayed in Figure 7a. while Figure 7b. displays the histogram for the output of the SPV units, it can be obvious that the output of the SPV has stochastic nature because of the change in solar irradiance. The cost factors of RESs for direct, penalty, and reserve costs are presented in Table 7.

Table 8 provides a comprehensive overview of the cost and emission coefficients utilized in the calculations pertaining to the thermal generating units.

The ACGO technique is used in this case to solve the optimal power flow framework considering stochastic RES as follows:

a) Case 1: Optimizing Fuel Cost with RES

Based on Eq.11, optimal scheduling of both thermal units, WT and SPV units for decreasing the total cost is achieved in this case. Table 9 presents the achieved optimal control variables with integrating RES to the system. The attained results indicate that the ACGO technique is more effective in solving the OPF problem than the original AEO and CGO techniques, producing superior results. Specifically, the total cost achieved by the ACGO algorithm in this scenario is $781.1675/h, outperforming the AEO and CGO techniques. The convergence characteristics of the ACGO approaches are depicted in Figure 8, with the ACGO algorithm demonstrating a smooth and rapid convergence. Figure 9 presents the boxplots of these techniques for case 1. Furthermore, Figure 10 illustrates the voltage profiles of the ACGO, AEO and CGO techniques. The voltage magnitudes for both techniques remain within the specified limits; however, the proposed ACGO algorithm exhibits

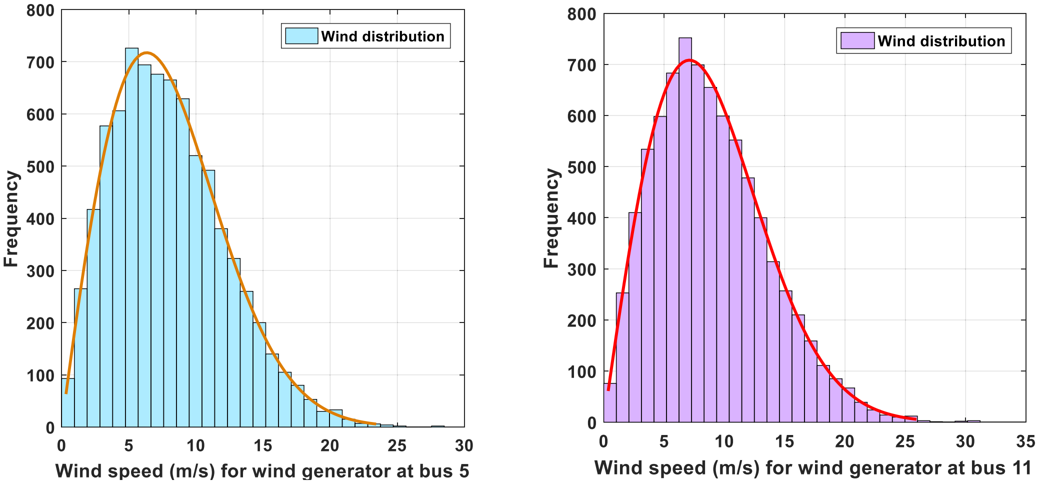

(a) (b)

FIGURE 6. Wind speed distribution for WT units.

TABLE 7. Energy source cost factor of the RES for the modified IEEE 30-bus and 57-bus systems.

Cost factor for RES	modified IEEE 30-bus system			modified IEEE 57-bus system	
	Wind power generating stations		Solar PV plant	Wind power generating stations	
	(bus 5)	(bus 11)	(bus 13)	(bus 6)	(bus 9)
Direct cost factor	1.6	1.75	1.6	1.6	1.75
Penalty cost factor	1.5	1.5	1.5	1.5	1.5
Reserve cost factor	3	3	3	3	3

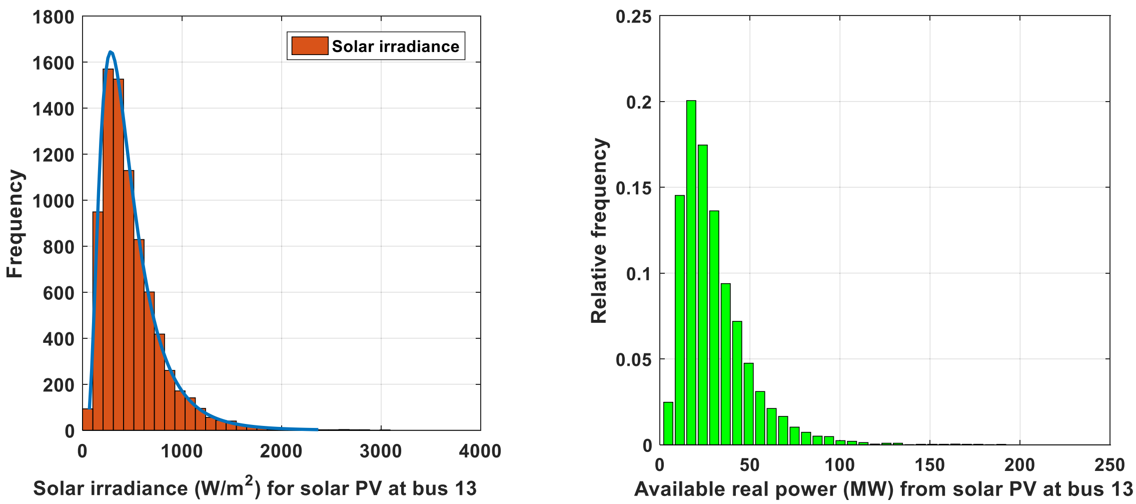

(a) Solar irradiance distribution (b) Active power distribution

FIGURE 7. Solar irradiance distribution and Active power distribution for SPV generators at bus13.

TABLE 8. Cost and emission coefficients of thermal generators for the system under study.

Generator	Bus	α	β	γ	e	g	a	b	c	ω	μ
P_{G1}	1	0	2	0.00375	18	0.037	4.091	-5.554	6.49	0.0002	6.667
P_{G2}	2	0	1.75	0.0175	16	0.038	2.543	-6.047	5.638	0.0005	3.333
P_{G8}	8	0	3.25	0.00834	12	0.045	5.326	-3.55	3.38	0.002	2

TABLE 9. Results of ACGO, AEO and CGO techniques for case 1.

	Min	Max	ACGO	AEO	CGO
Generator active power					
P_{G1}(MW)	50	200	134.9079	134.9825	134.9076
P_{G2}(MW)	20	80	27.97231	28.81275	27.39745
P_{W1}(MW)	0	75	44.29781	43.53096	43.20813
P_{G8}(MW)	10	35	10	10.01511	10.0009
P_{W2}(MW)	0	60	37.25461	37.03983	36.52928
P_{S1}(MW)	0	50	34.71403	34.86604	37.14496
Generator voltage					
V_1(p.u.)	0.95	1.1	1.071966	1.070816	1.071508
V_2(p.u.)	0.95	1.1	1.056848	1.056094	1.056308
V_5 (p.u.)	0.95	1.1	1.03494	1.073973	1.035045
V_8 (p.u.)	0.95	1.1	1.054964	1.038623	1.051103
V_{11} (p.u.)	0.95	1.1	1.098886	1.082645	1.097989
V_{13} (p.u.)	0.95	1.1	1.047368	1.063722	1.04873
Objective function					
Fuel cost ($/h)			781.1675	781.8781	782.0531
Fuel thermal unit cost			438.8182	441.9433	436.9234
Wind generation cost			249.2163	245.8096	242.9548
Solar generation cost			93.13306	94.12522	102.1749
Emission (ton/h)			1.762212	1.770122	1.762326
Total cost ($/h)			-	-	
Carbon tax ($/h)			-	-	
Power loss (MW)			5.746672	5.84715	5.788374
Voltage deviation (p.u.)			0.451471	0.465936	0.454008
Time (s)			863.3326	406.6191	701.7927
Generator reactive power					
Q_{G1}(MVAR)	-20	150	-1.83629	-3.04441	-2.00742
Q_{G2}(MVAR)	-20	60	11.80551	6.405404	10.84664
Q_{W1}(MVAR)	-30	35	22.39939	35	23.16602
Q_{G8}(MVAR)	-15	40	40	32.58794	40
Q_{W2}(MVAR)	-25	30	30	24.21354	30
Q_{S1}(MVAR)	-20	25	14.58153	21.60789	15.04427

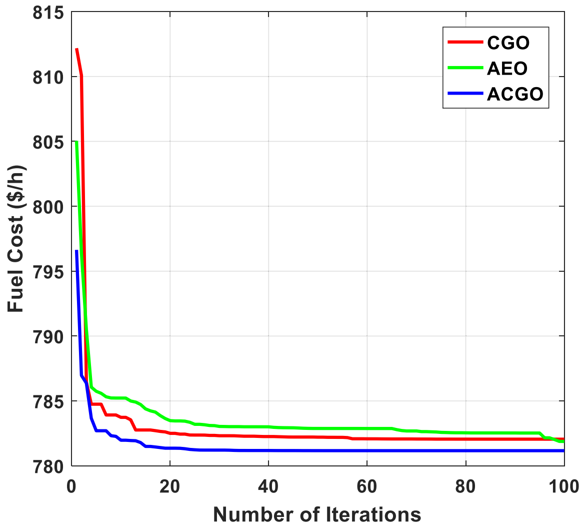

FIGURE 8. Convergence curves of the studied techniques for the first case.

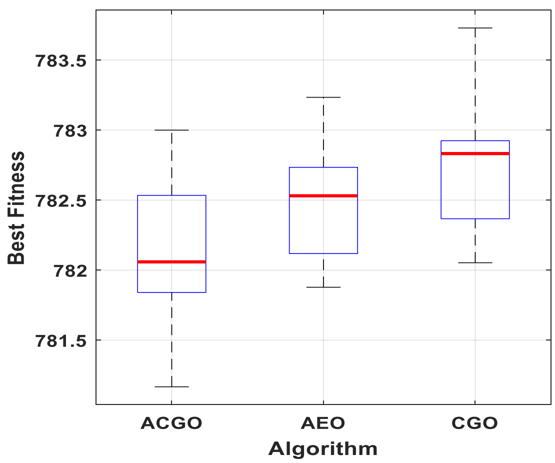

FIGURE 9. Boxplots of the studied techniques for the first case.

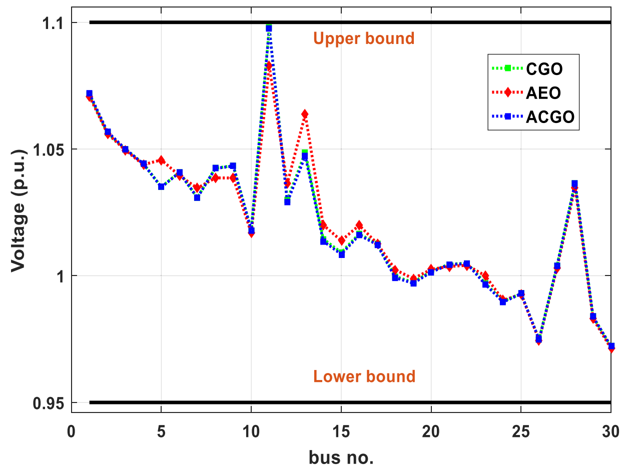

FIGURE 10. Voltage magnitude of the studied techniques for the first case.

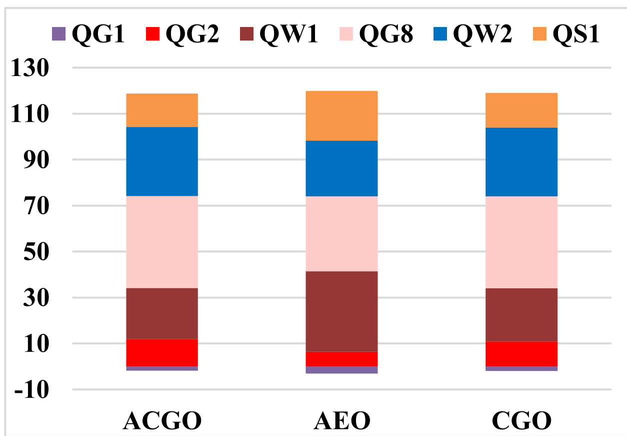

FIGURE 11. Representation of reactive power generation for the first case.

a better voltage profile compared to the AEO and CGO techniques. Figure 11 presents the reactive power of units for all algorithms. For this case, Statistical results the studied algorithms ACGO, AEO and CGO algorithms and previous researches are presented in Table 10. Moreover, Table 11 shows the comparison with these studied algorithms and previous researches in terms of fuel cost, emission, transmission losses, and voltage deviation values.

b) Case 2: Optimizing the Fuel cost with a carbon tax and RES.

Based on Eq.12 with incorporating RES, the ACGO technique is employed to reduce the total cost with the imposition of the CT. Additional, RES penetration is predicted to rise, and this is confirmed using the simulation results. Table 12 display the optimal solution achieved by the ACGO and AEO and CGO techniques for improving the power schedule of all parameters mandatory. Table 12 clearly shows that a higher penetration of RES has been attained in this scenario compared to case 2. The range of RES penetration in the optimal schedule is influenced by the number of CTs implemented and the level of emissions. Moreover, Figure 12 presents the convergence curves attained using the ACGO, AEO and CGO techniques for this scenario. It is evident that the ACGO algorithm delivers optimal performance in minimizing the total cost. Figure 13 shows the boxplot of the ACGO compared with the original AEO and CGO techniques for case 2. Also, Figure 14 presents the voltage profiles for the second case. For all voltage buses, they are inside definite limit. The reactive power of generators for all techniques is displayed in Figure 15.

Finally, Table 13 shows the statistical analysis achieved using several techniques as well the algorithm, including GOA, black widow optimization (BWO), GWO, ALO, PSO, GSA, MFO, BMO, Wild Horse Optimizer (WHO), elite evolutionary strategy Wild Horse Optimizer (EESWHO), AEO and CGO for the case 2. It is clear that the ACGO algorithm superiors these techniques from the previous literature as well as the conventional AEO and CGO algorithms for case 2. It is

TABLE 10. Statistical analysis the ACGO, AEO and CGO algorithms and previous researches for case 1.

Algorithm	Min.	Mean	Median	Max.	STD
ACGO	781.1675	782.1205	782.0595	782.9998	0.516074
AEO	781.8781	782.5193	782.5312	783.2341	0.452632
CGO	782.0531	782.7236	782.8325	783.7293	0.478367
WHO [18]	781.6866	782.1924	782.2067	782.7441	0.332675
EESWHO [18]	781.6322	782.3088	782.3227	782.8886	0.375421
GOA [46]	785.7109	804.0168	-	823.4731	9.52E+00
BWOA [46]	784.8148	788.2471	-	795.4683	5.83E+00
GWO [46]	781.6645	783.0412	-	783.3359	2.75E-01
ALO [46]	781.6562	784.3253	-	791.9234	2.49E+00
PSO [46]	781.9047	784.9048	-	794.4221	2.52E+00
GSA [46]	782.2237	785.8603	-	794.8996	2.43E+00
MFO [46]	781.6928	782.492	-	783.9305	4.77E-01
BMO [46]	781.6519	781.8187	-	783.5284	3.44E-01
CSA [47]	782.2001	782.5745	-	783.0720	0.1943
TLBO [47]	782.0373	782.3001	-	785.1228	0.5949
ABC [47]	782.0560	782.3940	-	784.8091	0.5875
EO [47]	782.0367	782.7271	-	789.3457	1.4318
IEO [47]	782.0343	782.0918	-	782.2878	0.0396

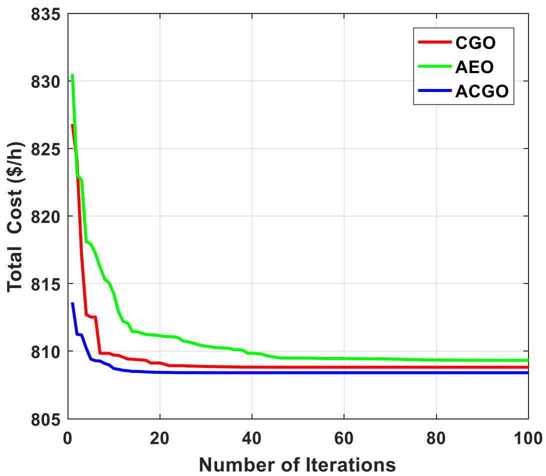

FIGURE 12. Convergence characteristic of the studied techniques for the second case.

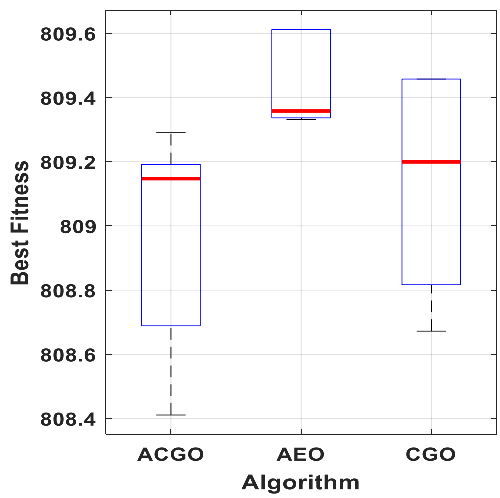

FIGURE 13. Boxplots of the studied techniques for the second case.

presented from this table that the proposed ACGO technique provides a best result in terms of precision and strength. Moreover, the results of well-known algorithms, such as EESWHO, WHO, JS, ABC, CGO, GPC, FPA, GA, CSA, SHADE-SF, GWO, PSO, MFO, MODE, and HPSO-GWO for the second case are shown in Table 14. Table 14 approves the effectiveness of the ACGO algorithm and demonstrates its

TABLE 11. Comparison of the ACGO, AEO and CGO algorithms and previous researches for case 1.

Method	Total cost ($/h)	Emission (t/h)	Ploss (MW)	VD (p.u.)
ACGO	781.1675	1.762212	5.746672	0.451471
AEO	781.8781	1.770122	5.84715	0.465936
CGO	782.0531	1.762326	5.788374	0.454008
GTO [12]	781.2626	1.76209	5.7117	0.4838
HGS [12]	781.86	1.7622	5.8460	0.48809
OPA [12]	782.076	1.76241	5.7882	0.46629
WHO [18]	781.6862	1.762122	5.796346	0.459112
EESWHO [18]	781.6322	1.762356	5.781681	0.453715
JS [48]	781.6387	1.761998	5.773893	0.448284
FPA [48]	782.8596	1.762312	5.863689	0.455137
GPC [48]	782.4229	1.764097	5.843226	0.537061
GA [35]	787.84	2.76	6.43	0.87
PSO [35]	785.82	2.36	6.79	1.08
CSA [35]	784.77	1.96	6.47	0.85
ABC [35]	783.81	1.75	6.06	0.56
GWO [35]	781.40	1.75	5.44	1.05
SHADE-SF [38]	782.503	1.762	5.77	0.463
CSA [47]	782.2001	-	6.0070	-
TLBO [47]	782.0373	-	5.9677	-
ABC [47]	782.0560	-	5.9554	-
EO [47]	782.0367	-	5.9545	-
IEO [47]	782.0343	-	5.9771	-

superiority on more than 10 well-known algorithms in various Scenarios of the OPF problem. The study demonstrates that the newly introduced hybrid overcomes the limitations of CGO, resulting in better performance of their hybrid approach. This modification suggests that the use of the hybrid approach can enhance the results of the basic algorithms. Thus, the suggested operator can potentially improve the performance of metaheuristics and other optimization techniques.

In Figure 16, a graphical representation is provided to illustrate the branch power flow analysis of two cases for the ACGO technique. The analysis is conducted on a modified IEEE 30-bus system, a well-known benchmark in power system research. The essential focus of this figure is to visually convey the results of power flow computations within specific branches of the system for the two cases considered. The power flow analysis is a fundamental aspect of power system studies, aimed at determining the distribution of electrical power across various components of the network. Overall, Figure 16 provides the branch power flow results generated by the ACGO technique for the modified IEEE 30-bus system. Its clear visualization aids in the assessment of the algorithm's performance and its ability to maintain branch power flow within acceptable limits, crucial for confirming the stability and consistency of power systems.

2) THE MODIFIED IEEE-57 BUS TEST SYSTEM.

The modified IEEE 57-bus system, depicted in Figure 17, serves as the testbed for evaluating the performance of the proposed ACGO algorithm concerning global optimization and stability capabilities, particularly for larger systems. This IEEE 57-bus system comprises 7 thermal generators, 57 load

TABLE 12. Results of ACGO, AEO and CGO techniques for the second case.

	Min	Max	ACGO	AEO	CGO
Generator active power					
P_{G1}(MW)	50	200	125.1002	124.5187	125.1641
P_{G2}(MW)	20	80	32.47258	30.99093	32.64794
P_{W1}(MW)	0	75	45.74169	45.04678	45.84607
P_{G8}(MW)	10	35	10	10.00182	10.00003
P_{W2}(MW)	0	60	38.53033	38.03933	38.59177
P_{S1}(MW)	0	50	36.89621	40.14053	36.49114
Generator voltage					
V_1(p.u.)	0.95	1.1	1.070854	1.070817	1.070931
V_2(p.u.)	0.95	1.1	1.057147	1.057092	1.057256
V_5 (p.u.)	0.95	1.1	1.03591	1.035526	1.035926
V_8 (p.u.)	0.95	1.1	1.040314	1.038503	1.040285
V_{11} (p.u.)	0.95	1.1	1.099594	1.098494	1.099529
V_{13} (p.u.)	0.95	1.1	1.055675	1.060642	1.055473
Objective function					
Fuel cost ($/h)			790.9967	792.4907	792.1933
Fuel thermal unit cost			431.1944	424.8038	431.9439
Wind generation cost			258.7595	254.5695	259.3489
Solar generation cost			101.0428	113.1174	100.9005
Emission (ton/h)			0.97668	0.944492	0.980294
Total cost ($/h)			808.4109	809.331	808.8166
Carbon tax ($/h)			17.83	17.83	17.83
Power loss (MW)			5.340979	5.338097	5.341025
Voltage deviation (p.u.)			0.468277	0.479563	0.467746
Time (s)			845.4375	414.7183	720.8735
Generator reactive power					
Q_{G1}(MVAR)	-20	150	-2.5624	-2.42882	-2.58269
Q_{G2}(MVAR)	-20	60	12.42296	13.35537	12.62411
Q_{W1}(MVAR)	-30	35	22.99233	23.25799	22.91948
Q_{G8}(MVAR)	-15	40	35.28291	32.02507	35.24253
Q_{W2}(MVAR)	-25	30	30	30	30
Q_{S1}(MVAR)	-20	25	17.68917	19.65984	17.61896

TABLE 13. Statistical analysis of the ACGO, AEO and CGO algorithms for case 2.

Algorithm	Min.	Mean	Median	Max.	STD
ACGO	808.4109	808.9952	809.1471	809.2918	0.308817
AEO	809.331	809.4525	809.358	809.6118	0.13739
CGO	808.6722	809.1331	809.1993	809.4576	0.309329
WHO [18]	808.6027	808.9931	808.9555	809.4384	0.257042
EESWHO [18]	808.462	809.0209	809.0756	809.8487	0.413675
GOA [46]	822.3074	839.1499	-	857.8005	9.32E+00
BWOA [46]	821.4095	824.358	-	830.89	2.66E+00
GWO [46]	811.2516	811.4707	-	811.6266	1.26E-01
ALO [46]	811.4334	811.7083	-	814.2972	5.36E-01
PSO [46]	811.5916	812.7758	-	818.8017	1.43E+00
GSA [46]	811.5264	811.7708	-	813.3572	4.97E-01
MFO [46]	811.4229	811.7398	-	812.4613	3.42E-01
BMO [46]	810.7982	810.7739	-	811.1199	1.45E-01

TABLE 14. Comparison of the ACGO, AEO and CGO algorithms and previous researches for case 2.

Method	Total cost ($/h)	Emission (t/h)	Ploss (MW)	VD (p.u.)
ACGO	808.4109	0.97668	5.340979	0.468277
AEO	809.331	0.944492	5.338097	0.479563
CGO	808.6722	0.980294	5.341025	0.467746
WHO [18]	808.6027	0.967898	5.345815	0.459422
EESWHO [18]	808.462	0.991702	5.342809	0.467842
JS [48]	810.12101	0.89377	5.276	0.46884
FPA [48]	811.6664	0.923031	5.307636	0.465664
GPC [48]	810.324	0.916127	5.327113	0.507454
GA [35]	814.72	1.36	5.63	0.64
PSO [35]	811.49	0.98	5.46	0.48
CSA [35]	811.53	0.92	5.44	0.49
ABC [35]	811.26	0.89	5.31	0.47
GWO [35]	809.93	0.86	4.99	1.07
SHADE-SF [38]	810.346	0.891	5.276	0.469
MFO [49]	809.969	0.898	5.010	1.067
HPSO-GWO [45]	809.277	0.914	5.132	0.462

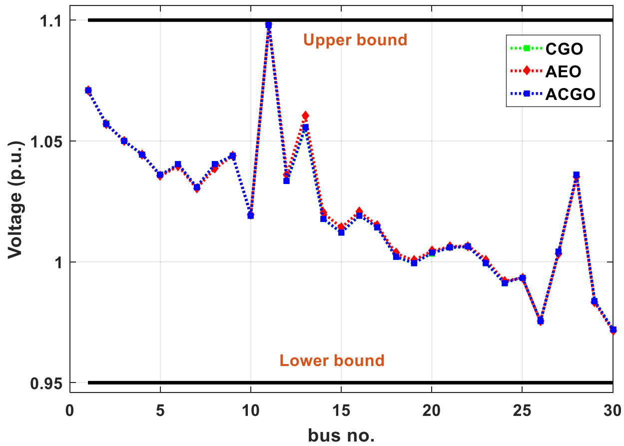

FIGURE 14. Voltage magnitude of the studied techniques for the second case.

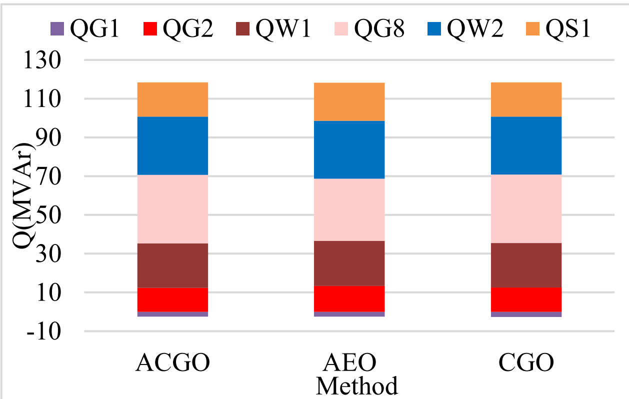

FIGURE 15. Representation of reactive power generation for the second case.

buses, 80 branches, 17 transformers, and 3 reactive power compensators. In this modified configuration, wind farms have replaced thermal power plants. Specifically, thermal power plants originally located at buses 1, 2, 3, 8, and 12, along with two wind farms comprising 50 and 40 wind turbines, have replaced thermal power stations at buses 6 and 9. You can find detailed data for the IEEE 57-bus system and parameters for the wind farms in Table 15. The wind power parameters for modified IEEE 57-bus system are provided in Table 16, while Table 17 contains information on the direct cost coefficients, penalty costs, and storage costs associated with Renewable Energy Sources (RES).

a: CASE 3: OPTIMIZING FUEL COST WITH RES

In Case 3, the fitness function aimed to decrease the overall cost, which comprised the fundamental thermal fuel cost and the wind-related expenses. In this case, the ACGO algorithm achieved a total cost value of $31,601.55 per hour. As indicated in Table 17, ACGO outperformed the original AEO and CGO algorithms in addressing this problem. Moreover, when compared to other algorithms, the difference in total cost became even more pronounced in the

TABLE 15. Analysis of the modified IEEE-57 bus system.

Item	Quantity	Details
No. of buses	57	[50]
No. of	80	[50]
Thermal	5	Buses; 1 (Slack), 3, 8, and 12
Wind	2	Buses; 6 and 9
Control variables	17	Tap changing transformer at branch (19, 20, 31, 35, 36, 37, 41, 46, 54, 58, 59, 65, 66, 71, 73, 76, 80)
	6	Scheduled actual power for 6 generators, including: Thg2, Thg3, Tg4, Tg5, WT1, and WT2
	7	The bus voltage of all generator
	3	Capacitor bank at branches 18, 25,
Connected	-	1250.8 MW, 336.4 MVAr
Load bus	24	[0.95 – 1.05] p.u.
Generator	6	[0.95 – 1.1] p.u.

modified IEEE 57-bus system, which is a larger and more complex power system compared to the IEEE 30-bus system. Specifically, the results obtained from the ACGO technique were $30.67 per hour cheaper than AEO and $5.68 per hour cheaper than CGO.

Figure 18 presents the convergence curves of the ACGO technique and other algorithms for the IEEE57-bus system with RES. Figure 19 presents the boxplots of these techniques for case 1. In Figure 20, you can see the voltage profiles of all buses in the results obtained from the ACGO, AEO, and CGO techniques for this case study. It's evident that the voltage values produced by the proposed ACGO and CGO algorithms all fall within the prescribed upper and lower limits. Additionally, Figure 21 displays the reactive power generated by the units for all these methods.

Table 18 presents significant findings obtained from the statistical analysis of the 57-bus system. Notably, the lowest standard deviation is observed in the case of ACGO, while the highest deviation is recorded in the PSO algorithm. The ranking clearly demonstrates that ACGO outperforms all other techniques. Additionally, Table 19 shows the comparison with these studied algorithms in terms of fuel cost, emission, transmission losses, and voltage deviation values.

b: CASE 4: OPTIMIZING THE FUEL COST WITH A CARBON TAX AND RES

In Case 4, the fitness function aimed to simultaneously decrease both the total cost and total emissions in an examination system comprising wind power and thermal generators. The carbon tax value in Equation (10) was set at 17.83. In this multi-objective scenario, the proposed ACGO algorithm yielded total cost and emissions values of $31,602.55 per hour and 1.175097 tons per hour,

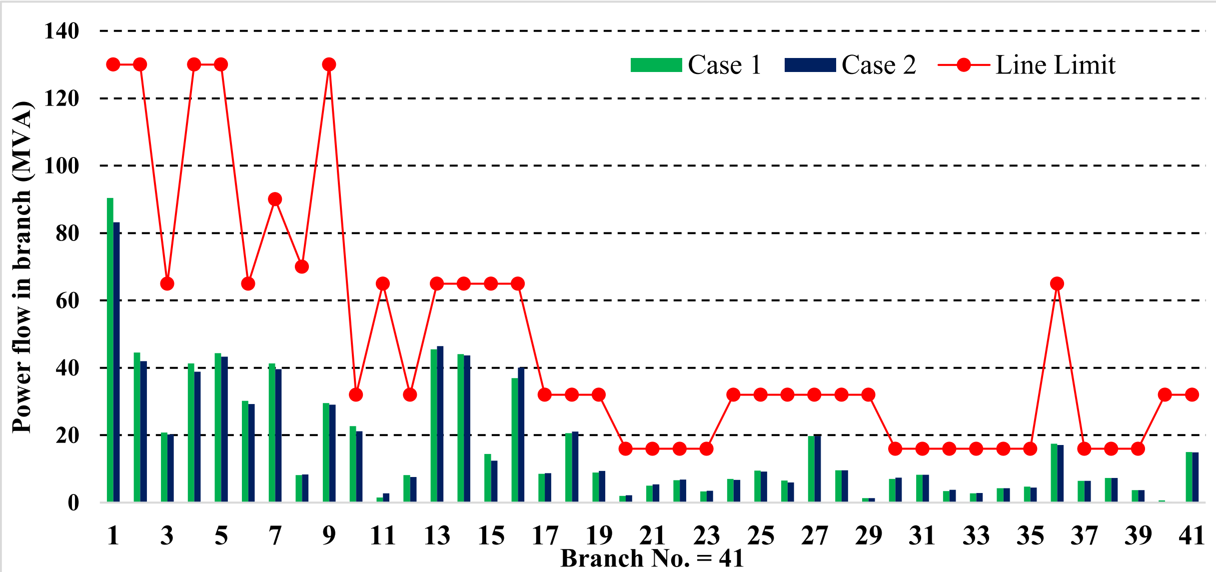

FIGURE 16. Power flow in branch of two cases of the proposed ACGO algorithm for the modified IEEE 30-bus system.

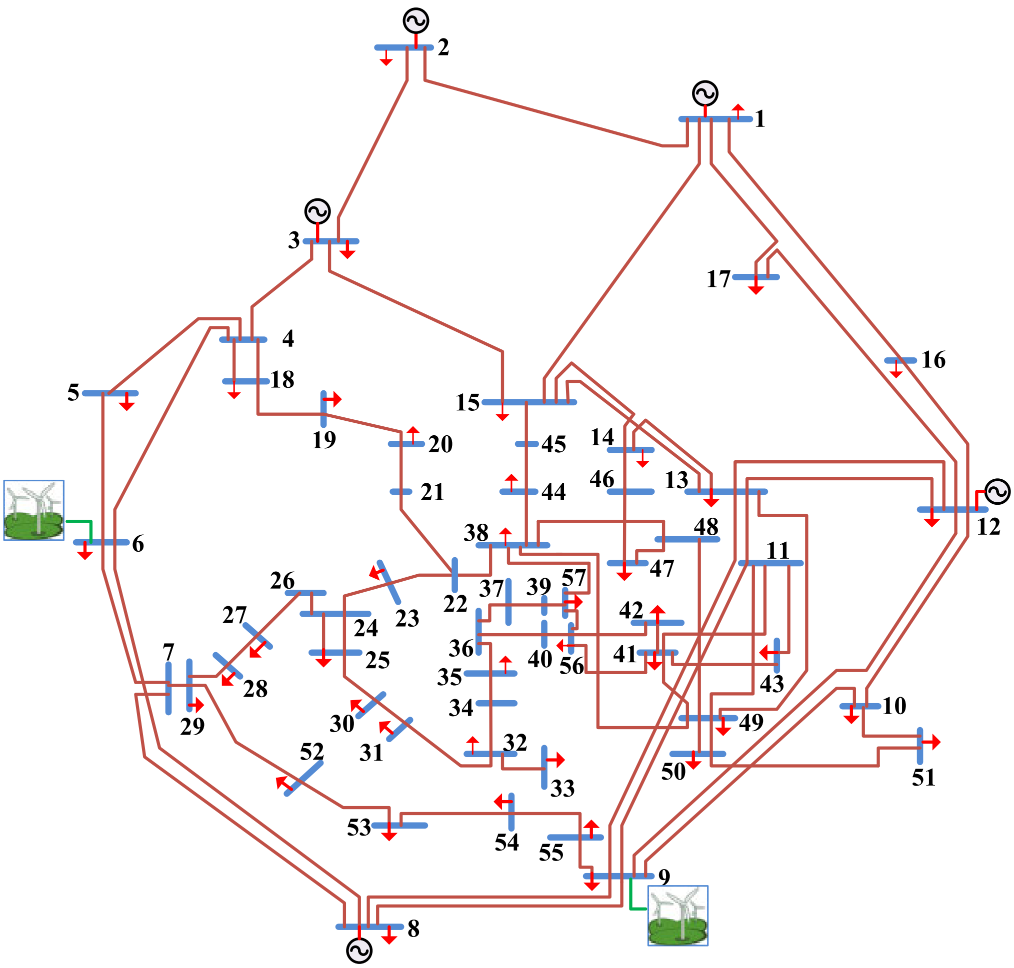

FIGURE 17. Modified IEEE 57-bus test system combined with wind energy.

TABLE 16. The parameters of wind power for the modified IEEE 57-bus test system.

Wind power generator units	q	vin (m/s)	vout (m/s)	vr (m/s)	k (m/s)	c (m/s)	Crwj	Cpwj	P_R (MW)	P_T (MW)
W6 (MW)	1.60	3	25	16	2	9	3	1.5	3	150
W9 (MW)	1.75	3	25	16	2	10	3	1.5	3	120

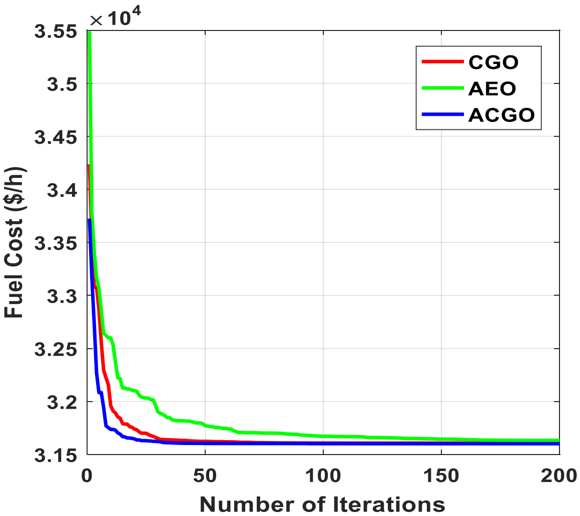

FIGURE 18. Convergence curves of the studied techniques for the third case.

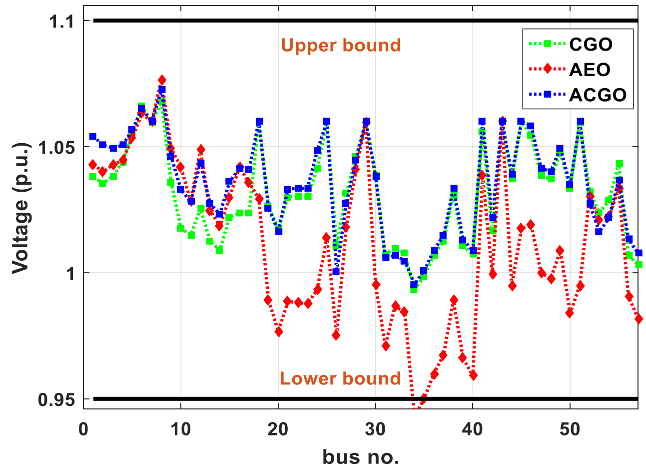

FIGURE 20. Voltage magnitude of the proposed algorithms for the third case.

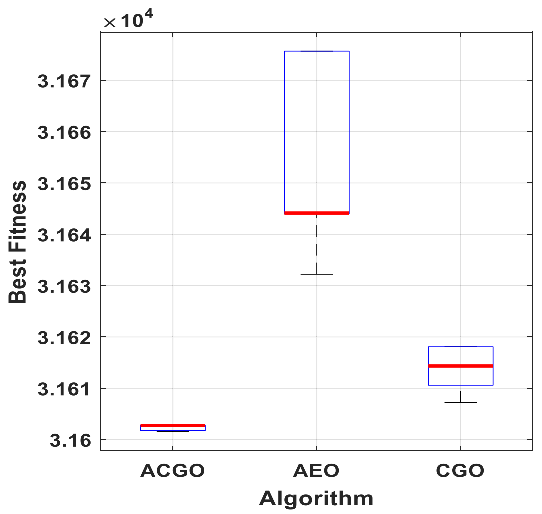

FIGURE 19. Boxplots of the studied techniques for the third case.

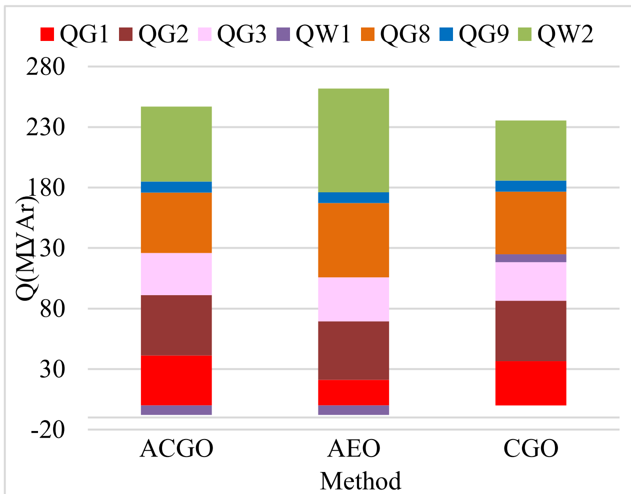

FIGURE 21. Representation of reactive power generation for the third case.

respectively. Referring to Table 20, the optimal fitness value achieved was $31,602.55 by ACGO, which was 16.41 lower than that obtained with AEO and 3.98 lower than CGO. In other words, for Case 4, ACGO outperformed the original AEO and CGO algorithms and emerged as the superior method.

The convergence curves of the original AEO, CGO techniques, and the ACGO technique are displayed in Figure 22, showing that the rapidity convergence of the ACGO algorithm was better than that of the AEO and CGO technique, i.e., the ACGO method was more effective in achieving an optimum solution compared to the other techniques for this test case. Figure 23 displays the boxplot of the ACGO method compared with the original AEO and CGO techniques for this study case. Figure 23's boxplots efficiently show the comparative performance of different algorithms for the fourth case, enabling researchers to make informed

TABLE 17. Results of the proposed ACGO, AEO, and CGO techniques for case 3.

	Min	Max	ACGO	AEO	CGO
Generator active power					
P_{G1}(MW)	0	576	136.8323	137.2494	136.4436
P_{G2}(MW)	30	100	50.26507	49.33095	49.26622
P_{G3}(MW)	40	140	42.55006	42.77133	42.34509
P_{W1}(MW)	0	150	150	149.9997	150
P_{G8}(MW)	100	550	424.5616	425.2841	425.0517
P_{W2}(MW)	0	120	120	119.9875	119.9997
P_{G12}(MW)	100	410	342.8016	343.1437	344.036
Generator voltage					
V_1(p.u.)	0.95	1.1	1.054105	1.042877	1.037962
V_2(p.u.)	0.95	1.1	1.050587	1.039988	1.035494
V_3 (p.u.)	0.95	1.1	1.049472	1.042802	1.038226
V_6(p.u.)	0.95	1.1	1.065014	1.063126	1.066141
V_8 (p.u.)	0.95	1.1	1.072497	1.076494	1.067837
V_9 (p.u.)	0.95	1.1	1.046036	1.049361	1.035647
V_{12} (p.u.)	0.95	1.1	1.043471	1.04872	1.025401
Capacitor bank					
Q_{C18} (MVAR)	0	20	11.68941	10.19297	14.48569
Q_{C25} (MVAR)	0	20	13.95626	3.814495	14.54313
Q_{C53} (MVAR)	0	20	11.55935	14.95478	14.16839
Transformer tap ratio					
T_{19}(4-18)	0.9	1.1	1.026148	0.990792	0.990208
T_{20}(4-18)	0.9	1.1	0.967597	1.02367	0.995019
T_{31}(21-20)	0.9	1.1	1.014794	1.01511	1.010129
T_{35}(24-25)	0.9	1.1	0.998959	0.970716	1.010372
T_{36}(24-25)	0.9	1.1	1.048979	0.945677	1.032162
T_{37}(24-26)	0.9	1.1	1.046253	1.019633	1.027788
T_{41}(7-29)	0.9	1.1	0.994767	0.992653	0.997033
T_{46}(34-32)	0.9	1.1	0.967739	0.919474	0.961353
T_{54}(11-41)	0.9	1.1	0.907535	0.956247	0.900938
T_{58}(15-45)	0.9	1.1	0.973502	1.007127	0.959226
T_{59}(14-46)	0.9	1.1	0.958272	0.987977	0.949003
T_{65}(10-51)	0.9	1.1	0.969491	1.044938	0.955074
T_{66}(13-49)	0.9	1.1	0.931751	0.94825	0.919399

TABLE 17. ***(Continued.)*** **Results of the proposed ACGO, AEO, and CGO techniques for case 3.**

T_{71}(11-43)	0.9	1.1	0.968	0.961098	0.954346
T_{73}(40-56)	0.9	1.1	0.994688	0.956772	1.013756
T_{76}(39-57)	0.9	1.1	0.968763	0.959499	0.96298
T_{80}(9-55)	0.9	1.1	1.004469	1.01305	0.989085
Objective function					
Fuel cost ($/h)			31601.55	31632.22	31607.23
Fuel thermal unit cost ($/h)			30672.28	30702.85	30677.97
Wind generation cost ($/h)			929.2591	929.2026	929.2577
Emission (ton/h)			1.176302	1.180316	1.18021
Total cost ($/h)			-	-	-
Carbon tax ($/h)			-	-	-
Power loss (MW)			16.21056	16.96662	16.34229
Voltage deviation (p.u.)			1.628727	1.277643	1.503967
L-index (max)			0.279764	0.295403	0.280748
Time (s)			1532.0745	851.5391	1350.9897
Generator reactive power					
Q_{G1}(MVAR)	-140	200	41.14068	21.13011	36.41666
Q_{G2}(MVAR)	-17	50	50	48.20555	50
Q_{G3}(MVAR)	-10	60	34.68457	36.54952	31.92558
Q_{G6}(MVAR)	-8	25	-7.99885	-8	6.618359
Q_{G8}(MVAR)	-140	200	50.01409	61.222	51.76305
Q_{G9}(MVAR)	-3	9	9	8.987536	8.977211
Q_{G12}(MVAR)	-150	155	61.94855	85.64647	49.62688

TABLE 18. **Statistical analysis of the ACGO, AEO and CGO algorithms for case 3.**

Algorithm	Min.	Mean	Median	Max.	STD
ACGO	31601.55	31602.33	31602.77	31602.76	0.550104
AEO	31632.22	31655.53	31644.14	31675.69	17.71742
CGO	31607.23	31614.01	31614.34	31618.09	4.415487
PSO [3]	33,400.326	34011.353	-	-	372.9083
GA [3]	31,637.539	31674.742	-	-	42.0234
MSA [3]	31,644.253	31678663	-	-	43.5123

decisions and draw insights about algorithm behavior and effectiveness within this specific scenario. Figure 24 displays the voltage profiles of all load buses for the ACGO, AEO and CGO techniques. The voltage magnitudes for both techniques remain within the specified limits. The reactive power of units for all techniques is presented in Figure 25. Moreover,

TABLE 19. Comparison of the ACGO, AEO and CGO algorithms and previous researches for case 3.

Method	Total cost ($/h)	Emission (t/h)	Ploss (MW)	VD (p.u.)
ACGO	31601.55	1.1763	16.2106	1.62873
AEO	31632.22	1.18032	16.9666	1.27764
CGO	31607.23	1.18021	16.3423	1.50397

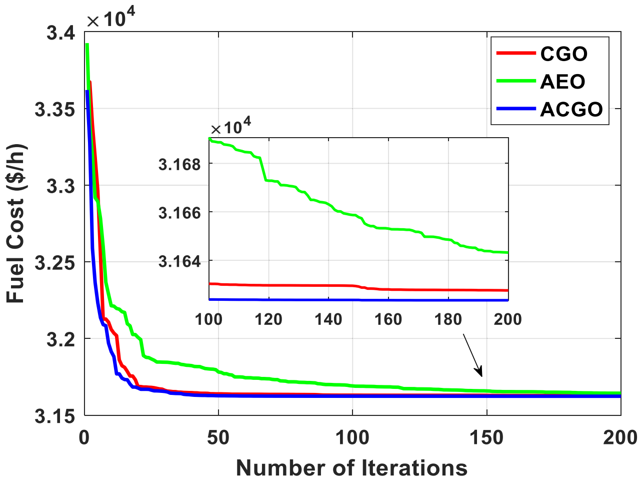

FIGURE 22. Convergence curves of the proposed techniques for the fourth case.

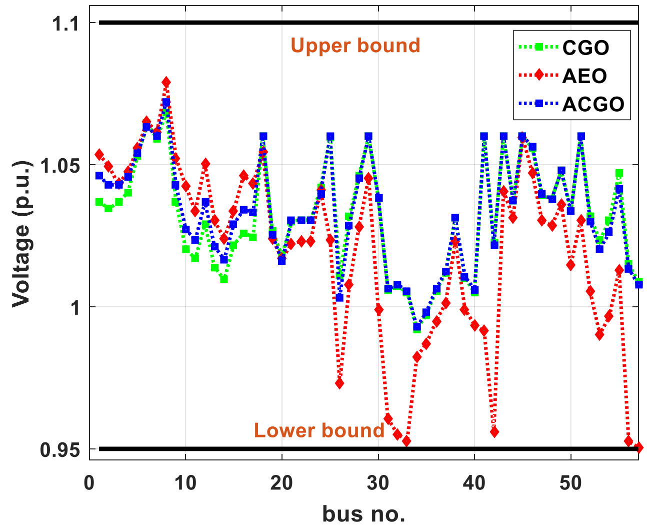

FIGURE 24. Voltage magnitude of the proposed algorithms for the fourth case.

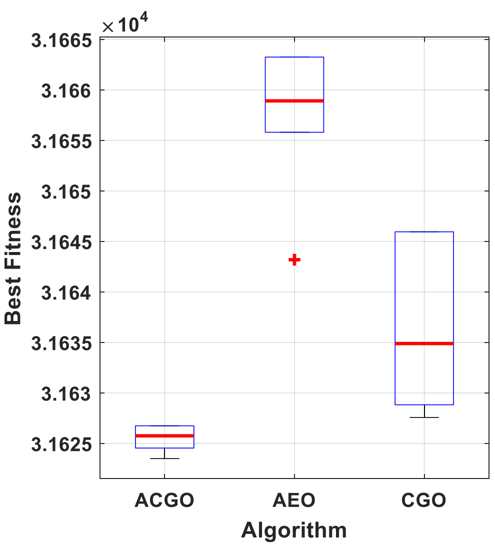

FIGURE 23. Boxplots of the proposed techniques for the fourth case.

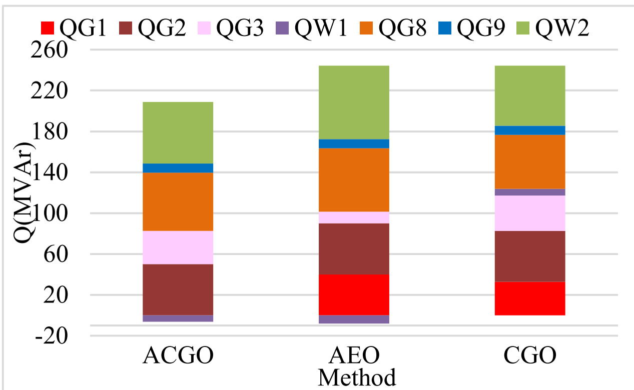

FIGURE 25. Representation of reactive power generation for the fourth case.

Figure 26 provides the branch power flow results generated by the proposed ACGO algorithm for the modified IEEE 57-bus system.

Table 21 presents key findings obtained from the statistical analysis of a 57-bus system for case 4. Especially, the ACGO algorithm demonstrates the smallest standard deviation, while the PSO algorithm exhibits the highest deviation in this case. The ranking indicates that ACGO surpasses all alternative methods in performance. Moreover, Table 22 provides a comprehensive contrast involving the studied algorithms, encompassing total cost, emissions, transmission losses, and voltage deviation metrics.

3) WILCOXON'S RANK TEST RESULTS

A nonparametric test, namely the WRST, was employed to establish the superiority of one technique over another.

TABLE 20. Results of the proposed ACGO, AEO, and CGO algorithms for case 4.

	Min	Max	ACGO	AEO	CGO
Generator active power					
P_{G1}(MW)	0	576	136.8447	138.3394	136.6458
P_{G2}(MW)	30	100	50.47125	48.27692	49.9888
P_{G3}(MW)	40	140	42.55322	42.2994	42.57477
P_{W1}(MW)	0	150	149.9999	149.9941	150
P_{G8}(MW)	100	550	424.1538	424.8172	424.7137
P_{W2}(MW)	0	120	120	119.9982	120
P_{G12}(MW)	100	410	342.9858	343.6797	343.2068
Generator voltage					
V_1(p.u.)	0.95	1.1	1.046027	1.053736	1.037038
V_2(p.u.)	0.95	1.1	1.042855	1.049561	1.034497
V_3 (p.u.)	0.95	1.1	1.042973	1.043189	1.036679
V_6(p.u.)	0.95	1.1	1.063466	1.065248	1.064558
V_8 (p.u.)	0.95	1.1	1.072267	1.078825	1.068296
V_9 (p.u.)	0.95	1.1	1.042741	1.052177	1.036922
V_{12} (p.u.)	0.95	1.1	1.036835	1.050309	1.02903
Capacitor bank					
Q_{C18} (MVAR)	0	20	11.78866	15.14528	8.808474
Q_{C25} (MVAR)	0	20	12.38277	14.64132	15.24207
Q_{C53} (MVAR)	0	20	12.766	8.195108	13.08379
Transformer tap ratio					
T_{19}(4-18)	0.9	1.1	0.982962	1.002167	0.906305
T_{20}(4-18)	0.9	1.1	0.991657	1.005247	1.038202
T_{31}(21-20)	0.9	1.1	1.01262	0.999591	1.009026
T_{35}(24-25)	0.9	1.1	1.01424	1.081854	1.069798
T_{36}(24-25)	0.9	1.1	0.996326	1.01342	0.982544
T_{37}(24-26)	0.9	1.1	1.03491	1.069631	1.027953
T_{41}(7-29)	0.9	1.1	0.995752	1.006082	0.996504
T_{46}(34-32)	0.9	1.1	0.963538	1.011474	0.963975
T_{54}(11-41)	0.9	1.1	0.903548	1.075188	0.900378
T_{58}(15-45)	0.9	1.1	0.965894	0.967762	0.959089
T_{59}(14-46)	0.9	1.1	0.953543	0.96917	0.947876
T_{65}(10-51)	0.9	1.1	0.963945	1.008789	0.957401
T_{66}(13-49)	0.9	1.1	0.927428	0.943882	0.919926

TABLE 20. ***(Continued.)*** **Results of the proposed ACGO, AEO, and CGO algorithms for case 4.**

T_{71}(11-43)	0.9	1.1	0.96345	0.97376	0.957501
T_{73}(40-56)	0.9	1.1	0.991322	1.022995	0.981205
T_{76}(39-57)	0.9	1.1	0.96642	0.994247	0.967702
T_{80}(9-55)	0.9	1.1	0.997099	1.033516	0.985803
Objective function					
Fuel cost ($/h)			31602.55	31618.96	31606.53
Fuel thermal unit cost ($/h)			30673.29	30689.73	30677.27
Wind generation cost ($/h)			929.2586	929.2252	929.2591
Emission (ton/h)			1.175097	1.180981	1.177471
Total cost ($/h)			31623.5	31643.19	31627.57
Carbon tax ($/h)			17.83	17.83	17.83
Power loss (MW)			16.2086	16.60496	16.32976
Voltage deviation (p.u.)			1.561689	1.452915	1.533303
L-index (max)			0.279694	0.296932	0.28111
Time (s)			1492.7836	834.9603	1319.8047
Generator reactive power					
Q_{G1}(MVAR)	-140	200	37.65773	39.91407	32.64637
Q_{G2}(MVAR)	-17	50	50	50	50
Q_{G3}(MVAR)	-10	60	32.65162	11.42515	34.51875
Q_{G6}(MVAR)	-8	25	-6.31739	-8	6.688285
Q_{G8}(MVAR)	-140	200	56.97341	62.02661	52.73107
Q_{G9}(MVAR)	-3	9	8.999996	9	8.998135
Q_{G12}(MVAR)	-150	155	60.06396	71.97155	58.5713

TABLE 21. **Statistical analysis of the ACGO, AEO and CGO algorithms for the fourth case.**

Algorithm	Min.	Mean	Median	Max.	STD
ACGO	31623.5	31625.47	31625.76	31626.75	1.135028
AEO	31643.19	31657.71	31658.91	31663.25	5.943669
CGO	31627.57	31636.47	31634.89	31645.96	8.464399
PSO [3]	33,092.210	33902.833	-	-	560.6028
GA [3]	31,668.644	31698.924	-	-	23.4437
MSA [3]	31,650.378	31691.178	-	-	28.5285

In this subsection, a detailed statistical analysis was conducted using the WRST to examine the distinctions between ACGO and the other techniques. The results derived from the WRST provide clear evidence that

TABLE 22. Comparison of the ACGO, AEO and CGO algorithms and previous researches for case 4.

Method	Total cost ($/h)	Emission (t/h)	Ploss (MW)	VD (p.u.)
ACGO	31623.5	1.175097	16.2086	1.56169
AEO	31643.19	1.180981	16.605	1.45292
CGO	31627.57	1.177471	16.3298	1.5333

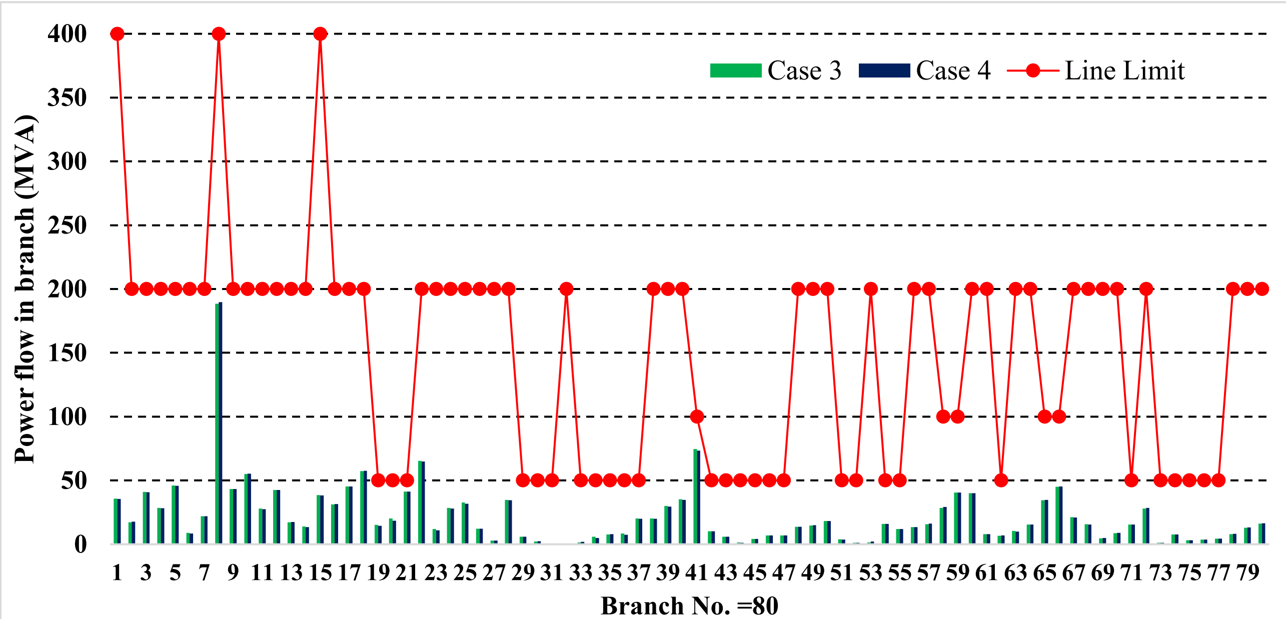

FIGURE 26. Power flow in branch of two scenarios of the ACGO techniques for the modified IEEE 57-bus system.

TABLE 23. Statistical results of the Wilcoxon rank-sum test.

ACGO vs	AEO		CGO	
Case no.	P	winner	P	winner
Case 1	6.4022E-02	=	1.7216E-02	+
Case 2	1.6494E-04	+	1.6039E-01	=
Case 3	1.2934E-04	+	1.2161E-04	+
Case 4	1.5932E-04	+	1.5748E-04	+
WRST (+/=/-)	3/1/0		3/1/0	

TABLE 24. Friedman test for the all-study cases of the proposed ACGO and other algorithms.

Case no.	ACGO	AEO	CGO
Case 1	1.2	2.1	2.7
Case 2	1.4	2.8	1.8
Case 3	1	3	2
Case 4	1	2.9	2.1
Mean ranks	1.15	2.7	2.15

ACGO surpasses the other proposed techniques, as depicted in Table 23.

4) FRIEDMAN'S RANK TEST RESULTS

Table 24 shows the statistical results attained using Friedman tests for the four test cases using the proposed ACGO, original AEO, and CGO algorithms. According to the results, the ranking of these approaches is as follows: ACGO, CGO, and AEO.

VI. CONCLUSION

The ACGO method has been formulated to enhance the optimization of the non-linear OPF problem. To validate its efficacy, the approach was implemented on seven numerical optimization test functions. Subsequently, the method was deployed to stochastic OPF solutions for two modified power networks (IEEE 30-bus and IEEE 57-bus systems) connected to RES. These stochastic OPF solutions were derived, accounting for uncertain solar and wind power generators. The objectives centered around minimizing both fuel costs and fuel costs in conjunction with total emissions. To illustrate the superiority of the ACGO algorithm, four scenarios were tested.

Within these scenarios, the OPF issue was simulated with the integration of renewable energy resources, utilizing the ACGO method to pinpoint the optimal control variables. It is seen that the ACGO approach exhibited exceptional performance, yielding the lowest fitness values of 781.1675 $/h and 808.4109 $/h in their respective cases for the modified IEEE 30-bus system. Also, the proposed ACGO method achieved the optimal total cost of 31623.5 $/h and 31601.55 $/h for the modified IEEE 57-bus system. These outcomes underscore the precision and robustness of the ACGO in efficiently tackling diverse instances of the OPF problem.

With the existence of RES, the ACGO technique outperformed other methodologies. It achieved the optimal total fuel cost of 781.1675 $/h, surpassing EESWHO (781.6322), WHO (781.6862 $/h), JS (781.6387 $/h), CGO (782.195 $/h), FPA (782.8596 $/h), and GPC (782.4229 $/h) for the first case. In the second scenario involving a carbon tax, the ACGO algorithm also demonstrated superior performance, attaining the lowest total cost of 808.4109 $/h. This again exceeded EESWHO (808.462 $/h), WHO (808.6027 $/h), JS (810.121 $/h), CGO (811.4568 $/h), FPA (811.6664 $/h), and GPC (810.324 $/h). These outcomes underscore the effectiveness of the ACGO technique in minimizing both total fuel costs and overall costs, even when factoring in carbon taxes, for the two systems (modified IEEE 30-bus and IEEE 57-bus) enriched with RES. Moreover, to validate the superiority of the ACGO technique over the existing algorithms, the attained results were compared with the results previously published in the related research work. In all examined cases, the ACGO algorithm emerged as the superior solution.

Statistical measures were employed to confirm the consistency and effectiveness of the technique. In forthcoming research endeavors, strides will be taken to enhance the ACGO algorithm's performance, particularly for larger-scale systems. Furthermore, the method will be extended to address the OPF problem while incorporating FACTS devices and other RES including hydrogen, fuel cells, and hydro generation.

ACKNOWLEDGMENT

This research has been funded by Scientific Research Deanship at University of Hail, Saudi Arabia, under project number RG-23 172.

REFERENCES

[1] R. Roy and H. T. Jadhav, "Optimal power flow solution of power system incorporating stochastic wind power using Gbest guided artificial bee colony algorithm," *Int. J. Electr. Power Energy Syst.*, vol. 64, pp. 562–578, Jan. 2015, doi: 10.1016/j.ijepes.2014.07.010.

[2] P. P. Biswas, P. N. Suganthan, R. Mallipeddi, and G. A. J. Amaratunga, "Optimal reactive power dispatch with uncertainties in load demand and renewable energy sources adopting scenario-based approach," *Appl. Soft Comput.*, vol. 75, pp. 616–632, Feb. 2019, doi: 10.1016/j.asoc.2018.11.042.

[3] E. Kaymaz, S. Duman, and U. Guvenc, "Optimal power flow solution with stochastic wind power using the Lévy coyote optimization algorithm," *Neural Comput. Appl.*, vol. 33, no. 12, pp. 6775–6804, Jun. 2021, doi: 10.1007/s00521-020-05455-9.

[4] M. A. Ali, S. Kamel, M. H. Hassan, E. M. Ahmed, and M. Alanazi, "Optimal power flow solution of power systems with renewable energy sources using white sharks algorithm," *Sustainability*, vol. 14, no. 10, p. 6049, May 2022, doi: 10.3390/su14106049.

[5] A. A. Mohamed, S. Kamel, M. H. Hassan, M. I. Mosaad, and M. Aljohani, "Optimal power flow analysis based on hybrid gradient-based optimizer with moth–flame optimization algorithm considering optimal placement and sizing of FACTS/wind power," *Mathematics*, vol. 10, no. 3, p. 361, Jan. 2022, doi: 10.3390/math10030361.

[6] M. A. M. Shaheen, H. M. Hasanien, S. F. Mekhamer, M. H. Qais, S. Alghuwainem, Z. Ullah, M. Tostado-Véliz, R. A. Turky, F. Jurado, and M. R. Elkadeem, "Probabilistic optimal power flow solution using a novel hybrid metaheuristic and machine learning algorithm," *Mathematics*, vol. 10, no. 17, p. 3036, Aug. 2022, doi: 10.3390/math10173036.

[7] M. H. Hassan, F. Daqaq, S. Kamel, A. G. Hussien, and H. M. Zawbaa, "An enhanced hunter-prey optimization for optimal power flow with FACTS devices and wind power integration," *IET Gener., Transmiss. Distrib.*, vol. 17, no. 14, pp. 3115–3139, Jul. 2023, doi: 10.1049/gtd2.12879.

[8] M. Rizwan, L. Hong, W. Muhammad, S. W. Azeem, and Y. Li, "Hybrid Harris hawks optimizer for integration of renewable energy sources considering stochastic behavior of energy sources," *Int. Trans. Electr. Energy Syst.*, vol. 31, no. 2, pp. 1–10, Feb. 2021, doi: 10.1002/2050-7038.12694.

[9] M. H. Hassan, S. Kamel, M. A. El-Dabah, T. Khurshaid, and J. L. Domínguez-García, "Optimal reactive power dispatch with time-varying demand and renewable energy uncertainty using Rao-3 algorithm," *IEEE Access*, vol. 9, pp. 23264–23283, 2021, doi: 10.1109/ACCESS.2021.3056423.

[10] S. Mouassa, F. Jurado, T. Bouktir, and M. A. Z. Raja, "Novel design of artificial ecosystem optimizer for large-scale optimal reactive power dispatch problem with application to Algerian electricity grid," *Neural Comput. Appl.*, vol. 33, no. 13, pp. 7467–7490, Jul. 2021, doi: 10.1007/s00521-020-05496-0.

[11] S. Mouassa, A. Althobaiti, F. Jurado, and S. S. M. Ghoneim, "Novel design of slim mould optimizer for the solution of optimal power flow problems incorporating intermittent sources: A case study of Algerian electricity grid," *IEEE Access*, vol. 10, pp. 22646–22661, 2022, doi: 10.1109/ACCESS.2022.3152557.

[12] S. Mouassa, S. Makhloufi, C. Djabali, and F. Jurado, "Optimal power flow solution based on gorilla troops optimization technique considering uncertainty of renewable energy sources: A case study of Adrar's isolated power network," *Wind Eng.*, vol. 47, no. 5, pp. 913–934, Oct. 2023, doi: 10.1177/0309524X231163826.

[13] S. Duman, S. Rivera, J. Li, and L. Wu, "Optimal power flow of power systems with controllable wind-photovoltaic energy systems via differential evolutionary particle swarm optimization," *Int. Trans. Electr. Energy Syst.*, vol. 30, no. 4, pp. 1–12, Apr. 2020, doi: 10.1002/2050-7038.12270.

[14] E. H. Houssein, M. H. Hassan, M. A. Mahdy, and S. Kamel, "Development and application of equilibrium optimizer for optimal power flow calculation of power system," *Appl. Intell.*, vol. 53, no. 6, pp. 7232–7253, Mar. 2023, doi: 10.1007/s10489-022-03796-7.

[15] M. H. Sulaiman and Z. Mustaffa, "An application of improved SALP swarm algorithm for optimal power flow solution considering stochastic solar power generation," *E-Prime-Adv. Electr. Eng., Electron. Energy*, vol. 5, Sep. 2023, Art. no. 100195, doi: 10.1016/j.prime.2023.100195.

[16] M. H. Hassan, S. Kamel, A. Selim, T. Khurshaid, and J. L. Domínguez-García, "A modified Rao-2 algorithm for optimal power flow incorporating renewable energy sources," *Mathematics*, vol. 9, no. 13, p. 1532, Jun. 2021, doi: 10.3390/math9131532.

[17] T. Samakpong, W. Ongsakul, and N. M. Manjiparambil, "Optimal power flow incorporating renewable uncertainty related opportunity costs," *Comput. Intell.*, vol. 38, no. 3, pp. 1057–1082, Jun. 2022, doi: 10.1111/coin.12316.

[18] M. H. Hassan, S. Kamel, and A. G. Hussien, "Optimal power flow analysis considering renewable energy resources uncertainty based on an improved wild horse optimizer," *IET Gener., Transmiss. Distrib.*, vol. 17, no. 16, pp. 3582–3606, Jun. 2023, doi: 10.1049/gtd2.12900.

[19] F. Daqaq, M. Ouassaid, S. Kamel, R. Ellaia, and M. F. El-Naggar, "A novel chaotic flower pollination algorithm for function optimization and constrained optimal power flow considering renewable energy sources," *Frontiers Energy Res.*, vol. 10, pp. 1–12, Sep. 2022, doi: 10.3389/fenrg.2022.941705.

[20] W. Zhao, L. Wang, and Z. Zhang, "Artificial ecosystem-based optimization: A novel nature-inspired meta-heuristic algorithm," *Neural Comput. Appl.*, vol. 32, no. 13, pp. 9383–9425, Jul. 2020, doi: 10.1007/s00521-019-04452-x.

[21] S. Talatahari and M. Azizi, "Chaos game optimization: A novel metaheuristic algorithm," *Artif. Intell. Rev.*, vol. 54, no. 2, pp. 917–1004, Feb. 2021, doi: 10.1007/s10462-020-09867-w.

[22] Y. Ma and Y. Bai, "A multi-population differential evolution with best-random mutation strategy for large-scale global optimization," *Appl. Intell.*, vol. 50, no. 5, pp. 1510–1526, May 2020, doi: 10.1007/s10489-019-01613-2.

[23] W. Ye, W. Feng, and S. Fan, "A novel multi-swarm particle swarm optimization with dynamic learning strategy," *Appl. Soft Comput.*, vol. 61, pp. 832–843, Dec. 2017, doi: 10.1016/j.asoc.2017.08.051.

[24] M. H. Hassan, S. Kamel, S. Q. Salih, T. Khurshaid, and M. Ebeed, "Developing chaotic artificial ecosystem-based optimization algorithm for combined economic emission dispatch," *IEEE Access*, vol. 9, pp. 51146–51165, 2021, doi: 10.1109/ACCESS.2021.3066914.

[25] B. A. Hassan, "CSCF: A chaotic sine cosine firefly algorithm for practical application problems," *Neural Comput. Appl.*, vol. 33, no. 12, pp. 7011–7030, Jun. 2021, doi: 10.1007/s00521-020-05474-6.

[26] J. Hu, H. Chen, A. A. Heidari, M. Wang, X. Zhang, Y. Chen, and Z. Pan, "Orthogonal learning covariance matrix for defects of grey wolf optimizer: Insights, balance, diversity, and feature selection," *Knowl.-Based Syst.*, vol. 213, Feb. 2021, Art. no. 106684, doi: 10.1016/j.knosys.2020.106684.

[27] L. Ma, S. Cheng, and Y. Shi, "Enhancing learning efficiency of brain storm optimization via orthogonal learning design," *IEEE Trans. Syst., Man, Cybern., Syst.*, vol. 51, no. 11, pp. 6723–6742, Nov. 2021, doi: 10.1109/TSMC.2020.2963943.

[28] W. Long, S. Cai, J. Jiao, M. Xu, and T. Wu, "A new hybrid algorithm based on grey wolf optimizer and cuckoo search for parameter extraction of solar photovoltaic models," *Energy Convers. Manage.*, vol. 203, Jan. 2020, Art. no. 112243, doi: 10.1016/j.enconman.2019.112243.

[29] M. H. Hassan, E. H. Houssein, M. A. Mahdy, and S. Kamel, "An improved Manta ray foraging optimizer for cost-effective emission dispatch problems," *Eng. Appl. Artif. Intell.*, vol. 100, Apr. 2021, Art. no. 104155, doi: 10.1016/j.engappai.2021.104155.

[30] S. M. J. Jalali, M. Ahmadian, S. Ahmadian, A. Khosravi, M. Alazab, and S. Nahavandi, "An oppositional-cauchy based GSK evolutionary algorithm with a novel deep ensemble reinforcement learning strategy for COVID-19 diagnosis," *Appl. Soft Comput.*, vol. 111, Nov. 2021, Art. no. 107675, doi: 10.1016/j.asoc.2021.107675.

[31] J. Xia, H. Zhang, R. Li, Z. Wang, Z. Cai, Z. Gu, H. Chen, and Z. Pan, "Adaptive barebones SALP swarm algorithm with quasi-oppositional learning for medical diagnosis systems: A comprehensive analysis," *J. Bionic Eng.*, vol. 19, no. 1, pp. 240–256, Jan. 2022, doi: 10.1007/s42235-021-00114-8.

[32] M. A. El-Dabah, M. H. Hassan, S. Kamel, and H. M. Zawbaa, "Robust parameters tuning of different power system stabilizers using a quantum artificial gorilla troops optimizer," *IEEE Access*, vol. 10, pp. 82560–82579, 2022, doi: 10.1109/ACCESS.2022.3195892.

[33] H. A. El-Sattar, S. Kamel, M. H. Hassan, and F. Jurado, "Optimal sizing of an off-grid hybrid photovoltaic/biomass gasifier/battery system using a quantum model of Runge Kutta algorithm," *Energy Convers. Manage.*, vol. 258, Apr. 2022, Art. no. 115539, doi: 10.1016/j.enconman.2022.115539.

[34] P. K. Adhvaryyu, P. K. Chattopadhyay, and A. Bhattacharya, "Dynamic optimal power flow of combined heat and power system with valve-point effect using Krill Herd algorithm," *Energy*, vol. 127, pp. 756–767, May 2017, doi: 10.1016/j.energy.2017.03.046.

[35] I. U. Khan, N. Javaid, K. A. A. Gamage, C. J. Taylor, S. Baig, and X. Ma, "Heuristic algorithm based optimal power flow model incorporating stochastic renewable energy sources," *IEEE Access*, vol. 8, pp. 148622–148643, 2020, doi: 10.1109/ACCESS.2020.3015473.

[36] H. M. Dubey, M. Pandit, and B. K. Panigrahi, "Hybrid flower pollination algorithm with time-varying fuzzy selection mechanism for wind integrated multi-objective dynamic economic dispatch," *Renew. Energy*, vol. 83, pp. 188–202, Nov. 2015, doi: 10.1016/j.renene.2015.04.034.

[37] S. S. Reddy and P. R. Bijwe, "Real time economic dispatch considering renewable energy resources," *Renew. Energy*, vol. 83, pp. 1215–1226, Nov. 2015, doi: 10.1016/j.renene.2015.06.011.

[38] P. P. Biswas, P. N. Suganthan, and G. A. J. Amaratunga, "Optimal power flow solutions incorporating stochastic wind and solar power," *Energy Convers. Manage.*, vol. 148, pp. 1194–1207, Sep. 2017, doi: 10.1016/j.enconman.2017.06.071.

[39] H. Youssef, S. Kamel, M. H. Hassan, and L. Nasrat, "Optimizing energy consumption patterns of smart home using a developed elite evolutionary strategy artificial ecosystem optimization algorithm," *Energy*, vol. 278, Sep. 2023, Art. no. 127793, doi: 10.1016/j.energy.2023.127793.

[40] A. M. Abd-El Wahab, S. Kamel, M. H. Hassan, J. L. Domínguez-García, and L. Nasrat, "Jaya-AEO: An innovative hybrid optimizer for reactive power dispatch optimization in power systems," *Electric Power Compon. Syst.*, vol. 2023, pp. 1–23, Jul. 2023, doi: 10.1080/15325008.2023.2227176.

[41] I. Ahmadianfar, O. Bozorg-Haddad, and X. Chu, "Gradient-based optimizer: A new metaheuristic optimization algorithm," *Inf. Sci.*, vol. 540, pp. 131–159, Nov. 2020, doi: 10.1016/j.ins.2020.06.037.

[42] I. Ahmadianfar, A. A. Heidari, S. Noshadian, H. Chen, and A. H. Gandomi, "INFO: An efficient optimization algorithm based on weighted mean of vectors," *Expert Syst. Appl.*, vol. 195, Jun. 2022, Art. no. 116516, doi: 10.1016/j.eswa.2022.116516.

[43] M. Dehghani, Š. Hubálovský, and P. Trojovský, "Northern goshawk optimization: A new swarm-based algorithm for solving optimization problems," *IEEE Access*, vol. 9, pp. 162059–162080, 2021, doi: 10.1109/ACCESS.2021.3133286.

[44] Y. Wang, P. Wang, J. Zhang, Z. Cui, X. Cai, W. Zhang, and J. Chen, "A novel bat algorithm with multiple strategies coupling for numerical optimization," *Mathematics*, vol. 7, no. 2, p. 135, Feb. 2019, doi: 10.3390/math7020135.

[45] M. Riaz, A. Hanif, S. J. Hussain, M. I. Memon, M. U. Ali, and A. Zafar, "An optimization-based strategy for solving optimal power flow problems in a power system integrated with stochastic solar and wind power energy," *Appl. Sci.*, vol. 11, no. 15, p. 6883, Jul. 2021, doi: 10.3390/app11156883.

[46] M. H. Sulaiman and Z. Mustaffa, "Optimal power flow incorporating stochastic wind and solar generation by metaheuristic optimizers," *Microsyst. Technol.*, vol. 27, no. 9, pp. 3263–3277, Sep. 2021, doi: 10.1007/s00542-020-05046-7.

[47] N. A. Nguyen, D. N. Vo, T. T. Nguyen, and T. L. Duong, "An improved equilibrium optimizer algorithm for solving optimal power flow problem with penetration of wind and solar energy," *Int. Trans. Electr. Energy Syst.*, vol. 2022, pp. 1–21, Jun. 2022, doi: 10.1155/2022/7827164.

[48] M. Farhat, S. Kamel, A. M. Atallah, and B. Khan, "Optimal power flow solution based on jellyfish search optimization considering uncertainty of renewable energy sources," *IEEE Access*, vol. 9, pp. 100911–100933, 2021, doi: 10.1109/ACCESS.2021.3097006.

[49] S. Pandya and H. R. Jariwala, "Single- and multiobjective optimal power flow with stochastic wind and solar power plants using moth flame optimization algorithm," *Smart Sci.*, vol. 10, no. 2, pp. 77–117, Apr. 2022, doi: 10.1080/23080477.2021.1964692.

[50] R. D. Zimmerman and C. E. Murillo-Sanchez. (2020). *MATPOWER*. Accessed: Aug. 31, 2023. [Online]. Available: https://matpower.org/

MOHAMED H. HASSAN received the B.Sc. degree (Hons.) in electrical engineering from Minia University, Egypt, in 2011, the M.Sc. degree in electrical engineering from Cairo University, Egypt, in 2018, and the joint Ph.D. degree from Aswan University, Egypt, and the University of Jaen, Spain, in 2022. He has published more than 60 papers in reputable journals and international conferences. His research interests include optimization techniques, power system analysis, renewable energy, and smart grids.

SALAH KAMEL received the international Ph.D. degree from Jaen University, Spain (Main), and Aalborg University, Denmark (Host), in January 2014. He is currently an Associate Professor with the Department of Electrical Engineering, Aswan University. He is also a Leader of the Advanced Power Systems Research Laboratory (APSR Lab), Power Systems Research Group, Aswan, Egypt. His research interests include power system analysis and optimization, smart grids, and renewable energy systems.

AYOOB ALATEEQ received the B.S. degree in electrical engineering from the University of Hail, Hail, Saudi Arabia, in 2009, and the M.S. and Ph.D. degrees from the University of Denver, in 2013 and 2018, respectively. He has been an Assistant Professor with the Department of Electrical Engineering, University of Hail, since 2019. His current research interest includes optimization in dc conversation.

ABDULLAH ALASSAF received the B.S. degree in electrical engineering from the University of Hail, Hail, Saudi Arabia, in 2013, and the M.S. and Ph.D. degrees in electrical engineering from the University of South Florida, Tampa, FL, USA, in 2017 and 2021, respectively. He is currently an Assistant Professor with the Department of Electrical Engineering, University of Hail. His current research interest includes power system dynamics and control.

IBRAHIM ALSALEH (Member, IEEE) received the B.S. degree in electrical engineering from the University of Hail, Hail, Saudi Arabia, in 2012, the M.S. and Ph.D. degrees in electrical engineering from the University of South Florida, Tampa, FL, USA, in 2016 and 2020, respectively. He is currently an Assistant Professor with the Department of Electrical Engineering, University of Hail. His current research interest includes optimization and reinforcement learning in smart power grids.